NACA RM L56J02

NACA

RESEARCH MEMORANDUM

HORIZONTAL-TAIL PARAMETERS AS DETERMINED FROM FLIGHT-TEST TAIL LOADS ON A FLEXIBLE SWEPT-WING JET BOMBER

By William S. Aiken, Jr., and Raymond A. Fisher

Langley Aeronautical Laboratory
Langley Field, Va.

NATIONAL ADVISORY COMMITTEE
FOR AERONAUTICS

WASHINGTON
January 17, 1957
Declassified September 13, 1957

NATIONAL ADVISORY COMMITTEE FOR AERONAUTICS

RESEARCH MEMORANDUM

HORIZONTAL-TAIL PARAMETERS AS DETERMINED FROM FLIGHT-TEST TAIL LOADS ON A FLEXIBLE SWEPT-WING JET BOMBER

By William S. Aiken, Jr., and Raymond A. Fisher

SUMMARY

An analysis is made of horizontal-tail loads on a flexible multi-engined jet-propelled swept-wing medium bomber to determine the following horizontal-tail parameters: tail lift-curve slope due to tail angle of attack $C_{l_{\alpha_t}}$, tail lift-curve slope due to elevator deflection C_{l_δ}, tail pitching-moment coefficient due to elevator deflection $C_{m_{\delta_t}}$, downwash factor $\frac{d\epsilon}{d\alpha}$, and the elevator effectiveness factor $\frac{d\alpha_t}{d\delta_e}$; and to determine the centers of pressure of loads due to angles of attack and elevator deflection. Comparison of the flight-determined parameters with available low-speed wind-tunnel data indicated excellent agreement, and the locations of the centers of pressure of the loads were in reasonable agreement with predictions. Least-squares curve-fitting procedures are used throughout the analysis, and a method is developed for determining zero shifts for the strain-gage-measured horizontal-tail loads.

INTRODUCTION

The calculation of aircraft longitudinal stability characteristics requires reliable estimates for such horizontal-tail parameters as tail lift-curve slope, elevator effectiveness, downwash factor, and tail pitching-moment coefficient due to elevator deflection. Recent tests made by the National Advisory Committee for Aeronautics which included measurements of horizontal-tail loads and fuselage deflections of a large flexible airplane permitted the analysis of data from which comparisons could be made between low-speed wind-tunnel parameters used in design and actual values as measured in flight.

The determination of the absolute values of tail loads measured by means of strain gages has been a particularly annoying problem because the strain-gage responses are sometimes seriously affected by structural temperature changes. The approach to the problem of correcting for temperature effects described in reference 1 was not adequate for the tail-load measurements reported herein because of the nature of the zero shifts which were present.

The present report has a twofold objective: (1) to analyze the tail loads measured in longitudinal maneuvers in terms of all existing angle-of-attack components at the tail and thus to obtain horizontal-tail parameters useful in estimating airplane response to specified elevator inputs, and (2) from these analyses for the conditions of zero tail angle of attack to determine the zero shift in the tail-loads measurements. Because the bending moments and torques as well as the shears on the tail were measured, the centers of pressure of the various components of tail load for the conditions of the tests are also given.

Descriptions are given of the methods used to account for fuselage flexibility effects and to obtain the necessary time-history data of tail angle-of-attack components. A description is also given of the procedure used for combining maneuvers for increased reliability of the coefficients. Least-squares procedures are used throughout the report, but because the procedures are relatively standardized no details are given.

SYMBOLS

A, B, C	tail-load coefficients for rigid fuselage conditions (defined by eqs. (8) and (9)), lb/deg
A_B, B_B, C_B, Z_B	tail bending-moment coefficients (defined by eq. (22))
A_T, B_T, C_T, Z_T	tail torque coefficients (defined by eq. (23))
A', B', C'	tail-load coefficients for flexible fuselage condition (defined by eq. (10)), lb/deg
$C_{T_{c/4}}$	tail-torque coefficient with tail 0.25 mean aerodynamic chord as reference station, in-lb/deg
K_1	change in tail incidence angle per unit aerodynamic tail load, deg/lb

K_2	change in tail incidence angle per unit tail load factor, deg/g units
L_{T_A}	horizontal tail aerodynamic load, lb
$L_{T_{A_C}}$	tail load corrected for zero shift (defined in eq. (24))
$L_{T_{struct}}$	structural horizontal-tail load, lb
M	Mach number
M_T	sum of left and right horizontal-tail root bending moments, in-lb
S_t	tail area, sq ft
T_T	total torque on horizontal tail with respect to strain-gage reference station, in-lb
V	true airspeed, ft/sec
W_t	weight of horizontal tail outboard of strain-gage reference station, lb
W_f	weight of fuel in rear fuselage tank, lb
Z	zero shift in measured tail load
Z'	a faired zero shift (defined by eq. (38))
a_F	airplane lift-curve slope (obtained from ref. 2), per degree
$\bar{c}_t$	tail mean aerodynamic chord, in.
g	acceleration of gravity, ft/sec^2
i_t	tail incidence angle, deg
i_w	wing incidence angle, deg
l_t	tail length, distance from airplane center of gravity to tail 0.25 mean-aerodynamic-chord location, positive forward, in.
n_t	tail normal-load factor, g units

Δn	increment in airplane normal-load factor at center of gravity (n - 1), g units
q	free-stream dynamic pressure, lb/sq ft
q_t	dynamic pressure at tail, lb/sq ft
x_α	chordwise center of pressure of load on tail due to angle-of-attack loads, in.
x_ϵ	chordwise center of pressure of load on tail due to downwash effected angle-of-attack loads, in.
x_δ	chordwise center of pressure of load on tail due to elevator deflection, in.
Δx	distance from strain-gage reference station to tail 0.25 mean aerodynamic chord, -9.7 in.
y_α	spanwise center of pressure of load on tail due to angle-of-attack loads, in.
y_ϵ	spanwise center of pressure of load on tail due to downwash effected angle-of-attack loads, in.
y_δ	spanwise center of pressure of load on tail due to elevator deflection
C_{L_t}	horizontal-tail lift coefficient
$C_{N_{A_C}}$	airplane normal-force coefficient corrected for pitching-acceleration tail load
$C_{m_{\delta_t}}$	tail pitching-moment coefficient about tail 0.25 mean aerodynamic chord due to elevator deflection, per radian
$c_{m_{\delta_{c/4}}}$	tail section pitching-moment coefficient about local quarter chord
$C_{l_{\alpha_t}}$	tail lift-curve slope with tail angle of attack, per degree
C_{l_δ}	tail lift-curve slope with elevator angle, per degree
α	angle of attack, deg

α_t	horizontal-tail angle of attack, deg
α_w	wing angle of attack, deg
$\alpha_{o_{adj}}$	airplane tail-on angle of zero lift with respect to fuselage reference line (from ref. 2), deg
α_1	tail angle-of-attack parameter (defined by eq. (19))
α_2	tail angle-of-attack parameter (defined by eq. (20))
$\dot{\alpha}$	time rate of change of angle of attack, deg/sec
$\dot{\gamma}$	time rate of change of flight-path angle, deg/sec
δ_e	elevator angle, deg
ϵ	downwash angle, deg
η_t	tail efficiency factor, q_t/q
$\dot{\theta}$	airplane pitching velocity, deg/sec
Λ	sweep angle of horizontal-tail quarter-chord line, deg
ρ	nondimensional strain-gage bridge response

APPARATUS AND TESTS

Airplane

The airplane used for this investigation was a six-engine, jet-propelled medium bomber. A photograph of the test airplane is shown in figure 1. The pertinent airplane characteristics and dimensions are given in table I.

Instrumentation

The data used for analysis in the present paper were obtained from standard NACA recording instruments and from strain gages mounted on the right and left sides of the horizontal tail. The recording instrumentation installed in the bomb bay of the test airplane is shown in figure 2.

Normal accelerations were measured by both single- and three-component air-damped accelerometers. Angular velocities in pitch were measured by a rate-gyro turnmeter which is magnetically damped. Elevator angles were measured by electrical resistance slide-type control position transmitters. Airspeed and altitude measurements were made with an NACA high-speed pitot-static head mounted on a boom approximately one maximum fuselage diameter ahead of the original nose.

Electrical wire-resistance strain gages with low-temperature correction factors were used to measure the root shears, bending moments, and torques at stations on the right and left sides of the tail. The gages were installed as four active arm bridges on the web and flanges of the main spars and on the upper and lower skin surfaces near the leading edges of the horizontal tail.

The strain-gage-bridge installation was calibrated according to the method detailed in reference 3. The bridges were then combined electrically so that, except for secondary carryover effects, a combined shear, moment, or torque bridge responded primarily to the shear, moment, or torque for the side of the tail on which the load was being measured.

The combined strain-gage outputs were recorded on an 18-channel oscillograph with individual galvanometer responses flat to 60 cycles per second. All data were evaluated by using nondimensional deflections as

$$\rho = \frac{\text{Flight deflection - Ground zero deflection}}{\text{Calibrate signal deflection}}$$

The sensitivity of each combined bridge was generally recorded prior to entering a maneuver through the use of a calibrate signal. With this system of data reduction, fluctuations in battery voltage had no effect on the measurement of loads. In addition, galvanometer zeros with strain-gage power off were recorded to compensate for any mechanical shifts in the galvanometer zero position due to temperature effects in the recorder and any thermal electromotive-force effects in the strain-gage circuits.

Aerodynamic tail loads on the horizontal tail were obtained from the structural loads (measured by the strain-gage bridges) and the known tail weight and normal-load factor from the equation

$$L_{T_A} = L_{T_{struct}} - n_t W_t$$

The aerodynamic bending moments and torques were obtained in a similar manner.

The recorded data for all instruments were synchronized at 0.1-second intervals by means of a common timing circuit. All instruments were damped to approximately 0.67 of critical damping. A summary of quantities measured, instrument locations, and accuracies are given in the following table:

Quantity Measured	Measurement station	Instrument range	Instrument accuracy
Normal acceleration, g units -			
Single component	34.2 percent wing M.A.C.	0 to 2	0.005
Three component	47.8 percent horiz.-tail root chord	-2 to 6	0.020
Pitching velocity, radians/sec	25 percent wing M.A.C.	±0.25	0.005
Elevator angle, deg	Elevator root	-22 to 12	0.075
Dynamic pressure, lb/sq ft	140 in. ahead of original nose	0 to 800	1
Static pressure, lb/sq ft	132 in. ahead of original nose	0 to 2,200	2
Tail shear, per side, lb	Root of tail	±25,000	60
Tail moment, per side, in-lb	Root of tail	±2,200,000	6,000
Tail torque, per side, in-lb	Root of tail	±2,000,000	4,000

Tests

All tests were made with the airplane in the clean condition. The flight data evaluated in this report were taken from 68 push-down, pull-up maneuvers (the same maneuvers used in ref. 2) made at altitudes of 20,000, 25,000, 30,000, and 35,000 feet and at an overall Mach number range from 0.427 to 0.812. The tests were made at normal and forward center-of-gravity positions and with airplane weights ranging from 104,000 to 127,000 pounds. Table II is a summary of the flight conditions for these tests. In the table are given the flight and run numbers, average Mach number, average dynamic pressure, test altitude, weight, and center-of-gravity position. Also, the Mach number and dynamic-pressure changes during any test run are indicated in the appropriate columns of table II.

METHOD

Horizontal-Tail Lift Parameters

In the following section the methods are developed by which the flight tail loads were analyzed and reduced to coefficient form. Basic rigid tail-load and angle-of-attack equations are modified as required to account for flexibility effects and to express the equations in forms suitable for analysis by least-squares procedures.

The horizontal-tail load is defined in terms of the tail angle of attack by the equation

$$L_{T_A} = \frac{dC_{L_t}}{d\alpha_t} \alpha_t \eta_t q S_t \tag{1}$$

where the tail angle of attack may be expressed as

$$\alpha_t = i_t - i_w + \alpha_w\left(1 - \frac{d\epsilon}{d\alpha}\right) - \dot{\alpha}\frac{l_t}{V}\frac{d\epsilon}{d\alpha} - \dot{\theta}\frac{l_t}{V}\frac{1}{\sqrt{\eta_t}} + \frac{d\alpha_t}{d\delta_e}\delta_e \tag{2}$$

The incidence of the test airplane tail is -0.25°, and the wing incidence is 2.75°. By assuming that $\eta_t = 1$ and using the relation

$$\dot{\alpha} = \dot{\theta} - \dot{\gamma} = \dot{\theta} - g\frac{\Delta n}{V} \tag{3}$$

equation (2) may be rewritten as

$$\alpha_t = -3.00 + \alpha_w\left(1 - \frac{d\epsilon}{d\alpha}\right) - \dot{\theta}\frac{l_t}{V}\frac{d\epsilon}{d\alpha} + g\frac{\Delta n l_t}{V^2}\frac{d\epsilon}{d\alpha} - \dot{\theta}\frac{l_t}{V} + \frac{d\alpha_t}{d\delta_e}\delta_e \tag{4}$$

By regrouping the terms of equation (4), the aerodynamic tail load for rigid conditions is obtained as

$$L_{T_A} = C_{l_{\alpha_t}} q S_t\left(\alpha_w - 3.00 - \dot{\theta}\frac{l_t}{V}\right) - \frac{d\epsilon}{d\alpha} C_{l_{\alpha_t}} q S_t\left(\alpha_w - g\frac{\Delta n l_t}{V^2} + \dot{\theta}\frac{l_t}{V}\right) + C_{l_\delta} q S_t \delta_e \tag{5}$$

Equation (5) is now in usable form for analysis of flight tail-load data when flexibility effects are unimportant. The necessary modifications to equation (5) to allow for proper handling of the effects of wing, tail, and fuselage flexibility follow.

Effects of flexibility.- The effect of wing flexibility on the angle of attack of the horizontal tail would be evident as the downwash behind the twisted wing changed with increasing wing-root angle of attack α_w. With constant values of dynamic pressure and Mach number during a symmetrical maneuver the downwash factor $\frac{d\epsilon}{d\alpha}$ would remain constant because the downwash and the wing twist would both be proportional to the change in wing-root angle of attack. Of course nonlinearities introduced by span loading changes near stall conditions would invalidate the linearity assumptions, but all data treated in the present report are well below stall conditions.

Horizontal stabilizer flexibility would produce changes in the tail lift-curve slope which for constant dynamic pressure and Mach number conditions would not affect the determination of the unknown coefficients of equation (5).

The effect of elevator flexibility which would be expected to be a function primarily of root elevator angle and dynamic pressure could also be determined for constant dynamic pressure and Mach number conditions if the root elevator angle is used in equation (5) for δ_e.

Thus the effects of wing, stabilizer, and elevator flexibility for quasi-static maneuvers would be evident in variations of $C_{l_{\alpha_t}}$, $\frac{d\epsilon}{d\alpha}$, and C_{l_δ} with dynamic pressure. For maneuvers made at constant q, they would be determinable from a least-squares analysis of time-history data by the use of equation (5) without modification.

The effect of fuselage flexibility on the tail coefficients is more difficult to assess because the fuselage bending deflection produces a change in angle of incidence of the horizontal tail which change is a function of the final balanced aerodynamic tail load and the inertia load on both the tail and the fuselage. Analysis of fuselage deflections measured during the subject tests, but not reported herein, indicated that the tail incidence angle due to fuselage deflections could be given accurately by the simple expression

$$i_{t,flex} = \frac{\partial i_t}{\partial L_{T_A}} L_{T_A} + \frac{\partial i_t}{\partial n_t} n_t \qquad (6)$$

where n_t is the normal acceleration at the tail. Analysis of the fuselage deflections measured in flight for various amounts of fuel in the rear fuselage fuel tanks indicated the numerical values pertinent to the test airplane to be given by the equation

$$i_{t,flex} = -\frac{0.578}{10^4}L_{T_A} + 0.250\left(1 + \frac{W_f}{10^4}\right)n_t \tag{7}$$

where the symbol W_f respresents the amount of fuel in pounds in the rear tank (the maximum value being approximately 14,000 pounds) during a particular maneuver.

If equation (6) is inserted into equation (5) as a tail incidence angle change there is then obtained

$$L_{T_A} = C_{l_{\alpha_t}} qS_t\left(\alpha_w - 3.00 + \frac{\partial i_t}{\partial L_{T_A}}L_{T_A} + \frac{\partial i_t}{\partial n_t}n_t - \dot{\theta}\frac{l_t}{V}\right) -$$

$$\frac{d\epsilon}{d\alpha}C_{l_{\alpha_t}} qS_t\left(\alpha_w - g\frac{\Delta n l_t}{V^2} + \dot{\theta}\frac{l_t}{V}\right) + C_{l_\delta} qS_t\delta_e \tag{8}$$

Although the term $\frac{\partial i_t}{\partial L_{T_A}}L_{T_A}$ may be computed from the data, any errors in L_{T_A} will be reflected in the parameters $C_{l_{\alpha_t}}$, $\frac{d\epsilon}{d\alpha}$, and C_{l_δ} of a least-squares solution of equation (8). Equation (8) may be rewritten as

$$L_{T_A} = A\left(\alpha_w - 3.00 + K_1 L_{T_A} + K_2 n_t - \dot{\theta}\frac{l_t}{V}\right) + B\left(\alpha_w - g\frac{\Delta n l_t}{V^2} + \dot{\theta}\frac{l_t}{V}\right) + C\delta_e \tag{9}$$

or, by regrouping the tail load terms, as

$$L_{T_A} = \frac{A}{1 - AK_1}\left(\alpha_w - 3.00 + K_2 n_t - \dot{\theta}\frac{l_t}{V}\right) + \frac{B}{1 - AK_1}\left(\alpha_w - g\frac{\Delta n l_t}{V^2} + \dot{\theta}\frac{l_t}{V}\right) + \frac{C}{1 - AK_1}\delta_e$$

or

$$L_{T_A} = A'\left(\alpha_w - 3.00 + K_2 n_t - \dot{\theta}\frac{l_t}{V}\right) + B'\left(\alpha_w - g\frac{\Delta n l_t}{V^2} + \dot{\theta}\frac{l_t}{V}\right) + C'\delta_e \tag{10}$$

Equations of the form of equation (10) may be used with time-history data to obtain values of the coefficients A', B', and C' by least-squares methods.

In order to obtain the correct values of $C_{l_{\alpha_t}}$, $\frac{d\epsilon}{d\alpha}$, and C_{l_δ} the coefficient A must first be calculated from the expression

$$\left.\begin{aligned} A' &= \frac{A}{1 - AK_1} \\ A &= \frac{A'}{1 + A'K_1} \end{aligned}\right\} \tag{11}$$

The values of the parameters $C_{l_{\alpha_t}}$, $\frac{d\epsilon}{d\alpha}$, C_{l_δ}, and $\frac{d\alpha_t}{d\delta_e}$ are then given by the equations

$$C_{l_{\alpha_t}} = \left(\frac{A'}{1 + A'K_1}\right)\left(\frac{1}{qS_t}\right) \tag{12}$$

$$\frac{d\epsilon}{d\alpha} = -B'/A' \tag{13}$$

$$C_{l_\delta} = \left(\frac{C'}{1 + A'K_1}\right)\left(\frac{1}{qS_t}\right) \tag{14}$$

$$\frac{d\alpha_t}{d\delta_e} = C'/A' \tag{15}$$

Time-history data.- For evaluating the A', B', and C' coefficients of equation (10), measurements of aerodynamic tail load, wing angle of attack, tail normal-load factor, pitching velocity and elevator angle are required in time-history form. As described in the section "Instrumentation" the aerodynamic tail loads were measured by using strain gages at the root of the horizontal tail. Tail and airplane normal-load factors and airplane pitching velocities were obtained from standard NACA recorders. The elevator angle used was the average of the left and right root elevator-angle measurements. The wing angle-of-attack time history was calculated from the equation

$$\alpha_w = \alpha_{o_{adj}} + \frac{1}{a_F} C_{N_{A_C}} + i_w \tag{16}$$

because, as pointed out in reference 2, the recorded angles of attack were often subject to a large amount of recorder lag. The values of $\alpha_{o_{adj}}$ and a_F were obtained from reference 2 for the tail-on conditions. The value of i_w is 2.75°, and time histories of $C_{N_{A_C}}$ were calculated by using equation (2) of reference 2. The use of calculated values of α_w (in addition to decreasing scatter due to recorder errors) provides a consistent set of angles of attack for the maneuvers to be analyzed which would be free of random errors in both angle of zero lift and lift-curve slope.

Tail-load zero shifts.- The time histories of the various tail angle-of-attack components could be used in equations of the form of equation (10) to determine by least squares the values of the A', B', and C' coefficients if the aerodynamic tail loads were completely free of zero shifts. Large zero shifts were present, and a preliminary analysis of these shifts indicated that they were apparently associated with the temperature of the skin strain gages mounted on the top and bottom of the stabilizer near the leading edge. The skin strain gages were covered by a small lens-like clear plastic covering as a protection against mechanical damage. Although no temperature measurements were available for this specific strain-gage location, the effect of temperature was determined by correlating motion pictures of the vertical and horizontal tail in straight, level flight with indicated strain-gage load dissymmetries. Although no usable quantitative results were obtained from this analysis, it was established that a shadow or lack of a shadow from the vertical tail on the top skin strain gages correlated directly with the direction and magnitude of the load dissymmetries. This correlation indicated that the stabilizer strain-gage installation was not adequate for directly determining absolute tail loads. Provision was made in the analysis of the data to determine the zero shift for each maneuver by adding a constant Z to equation (10) and letting a least-squares procedure establish its numerical value. The equation used for least-squares analysis thus becomes

$$L_{T_A} = Z + A'\left(\alpha_w - 3.00 + K_2 n_t - \dot{\theta}\frac{l_t}{V}\right) + B'\left(\alpha_w - g\frac{\Delta n l_t}{V^2} + \dot{\theta}\frac{l_t}{V}\right) + C'\delta_e \qquad (17)$$

Combination of maneuvers.- Although 68 different push-pull maneuvers were available for the present analysis, some of these maneuvers were made at approximately the same dynamic pressure and Mach number conditions. Since airplane weight and center-of-gravity position are not variables which affect the determination of the unknown aerodynamic coefficients of equation (17) two or three maneuvers at the same dynamic pressure and Mach number could be least squared together to produce

more reliable values of the A', B', and C' coefficients. The increased reliability results from an extension of the range of the variables and the improvement of the matrix solution by simultaneous fitting of time histories with difference shapes. The procedure of combining maneuvers is accomplished by allowing a zero shift coefficient as in equation (17) (for example, Z_1 and Z_2) for each run to represent the only independent parameter of the combined maneuvers. For example, the equation used for combining two maneuvers was

$$\begin{Bmatrix} \{L_{T_{A_1}}\} \\ \hline \{L_{T_{A_2}}\} \end{Bmatrix} = \left\| \begin{array}{ccccc} 1 & 0 & \alpha_1 & \alpha_2 & \delta_e \\ \cdot & \cdot & \cdot & \cdot & \cdot \\ \cdot & \cdot & \cdot & \cdot & \cdot \\ \cdot & \cdot & \cdot & \cdot & \cdot \\ \hline 0 & 1 & \alpha_1 & \alpha_2 & \delta_e \\ \cdot & \cdot & \cdot & \cdot & \cdot \\ \cdot & \cdot & \cdot & \cdot & \cdot \\ \cdot & \cdot & \cdot & \cdot & \cdot \end{array} \right\| \begin{Bmatrix} Z_1 \\ Z_2 \\ A' \\ B' \\ C' \end{Bmatrix} \tag{18}$$

where

$$\alpha_1 = \alpha_w - 3.00 + K_2 n_t - \dot{\theta}\frac{l_t}{V} \tag{19}$$

and

$$\alpha_2 = \alpha_w - g\frac{\Delta n l_t}{V^2} + \dot{\theta}\frac{l_t}{V} \tag{20}$$

An additional refinement was used in the analysis if the maneuvers were made at the same Mach number but at slightly different dynamic pressures. In this case equation (18) was written as

$$\begin{Bmatrix} \{L_{T_{A_1}}/q_1\} \\ \hline \{L_{T_{A_2}}/q_2\} \end{Bmatrix} = \left\| \begin{array}{ccccc} 1 & 0 & \alpha_1 & \alpha_2 & \delta_e \\ \cdot & \cdot & \cdot & \cdot & \cdot \\ \cdot & \cdot & \cdot & \cdot & \cdot \\ \cdot & \cdot & \cdot & \cdot & \cdot \\ \hline 0 & 1 & \alpha_1 & \alpha_2 & \delta_e \\ \cdot & \cdot & \cdot & \cdot & \cdot \\ \cdot & \cdot & \cdot & \cdot & \cdot \\ \cdot & \cdot & \cdot & \cdot & \cdot \end{array} \right\| \begin{Bmatrix} Z_1/q_1 \\ Z_2/q_2 \\ A'/q \\ B'/q \\ C'/q \end{Bmatrix} \tag{21}$$

and equation (21) was solved by least squares for the parameters of the column matrix on the right-hand side of the equation.

Horizontal-Tail Centers of Pressure

The horizontal-tail bending moments and torques were measured by use of strain gages so that the centers of pressure of the individual load components - such as the loads due to angle of attack, downwash, and elevator angle - could be evaluated separately. Since for the symmetrical maneuvers considered in the present analysis the effects of the small amount of roll and sideslip occurring during a maneuver were negligible, the aerodynamic bending moments and torques for the two sides were added together. The total bending moment M_T including moment-zero shifts was expressed by the equation

$$M_T = A_B\left(\alpha_w - 3.00 + K_1 L_{T_{A_C}} + K_2 n_t - \dot{\theta}\frac{l_t}{V}\right) +$$

$$B_B\left(\alpha_w - g\frac{\Delta n l_t}{V^2} + \dot{\theta}\frac{l_t}{V}\right) + C_B\delta_e + Z_B \qquad (22)$$

and the total torque - including torque-zero shifts - by the equation

$$T_T = A_T\left(\alpha_w - 3.00 + K_1 L_{T_{A_C}} + K_2 n_t - \dot{\theta}\frac{l_t}{V}\right) +$$

$$B_T\left(\alpha_w - g\frac{\Delta n l_t}{V^2} + \dot{\theta}\frac{l_t}{V}\right) + C_T\delta_e + Z_T \qquad (23)$$

It will be noted that the term for stabilizer angle of attack due to fuselage bending which is due to tail load $K_1 L_{T_{A_C}}$ is included in both equations (22) and (23). Since the tail load has presumably been fitted previously, the tail zero shift term Z may be accounted for in the moment and torque equations as

$$L_{T_{A_C}} = L_{T_A} - Z \qquad (24)$$

Thus solutions of equations of the form of equations (22) and (23) provide bending-moment and torque coefficients for the rigid fuselage case unaffected by zero shifts.

The solution of equations of the form of equations (22) and (23) by least squares using time-history data permitted the determination of the spanwise and chordwise centers of pressure with respect to the strain-gage reference station. The spanwise centers of pressure were determined from the equations

$$\left.\begin{aligned} y_\alpha &= A_B/A \\ y_\epsilon &= B_B/B \\ y_\delta &= C_B/C \end{aligned}\right\} \tag{25}$$

Similarly, the chordwise centers of pressure were determined from the equations

$$\left.\begin{aligned} x_\alpha &= A_T/A \\ x_\epsilon &= B_T/B \\ x_\delta &= C_T/C \end{aligned}\right\} \tag{26}$$

The coefficient A of the shear or load equation is given in equation (11) as

$$A = \frac{A'}{1 + A'K_1}$$

Similarly, the B and C coefficients are defined as

$$\left.\begin{aligned} B &= \frac{B'}{1 + A'K_1} \\ C &= \frac{C'}{1 + A'K_1} \end{aligned}\right\} \tag{27}$$

Tail Pitching-Moment Coefficient Due to Elevator Deflection

From the solution of equations of the form of equation (23), the coefficient C_T was used to determine $C_{m_{\delta_t}}$. Since C_T is defined

on the basis of an arbitrary reference station it was necessary to redefine it in terms of the tail 25-percent mean-aerodynamic-chord location by the equation

$$C_T = C_{T_{c/4}} + \Delta x C \tag{28}$$

where Δx is the distance from the strain-gage reference station to tail 0.25 mean aerodynamic chord. The equation defining $C_{m_{\delta_t}}$ is

$$C_{m_{\delta_t}} = \frac{C_{T_{c/4}}}{qS_t\bar{c}_t} \tag{29}$$

thus, $C_{m_{\delta_t}}$ was evaluated from

$$C_{m_{\delta_t}} = \left(\frac{C_T}{qS_t\bar{c}_t}\right)\left(1 - \frac{\Delta x}{x_\delta}\right) \tag{30}$$

For the present case the value of Δx is -9.7 inches, and values of x_δ are computed from equation (26).

RESULTS AND DISCUSSION

The preceding section has given the procedures used for obtaining the horizontal-tail lift-curve slope, the downwash parameter $\frac{d\epsilon}{d\alpha}$, the elevator effectiveness $\frac{d\alpha_t}{d\delta_e}$, the centers of pressures of the various loads on the tail, and the tail pitching-moment coefficient $C_{m_{\delta_t}}$ from time-history measurements of total shears, bending moments, and torques at the root of the horizontal stabilizer. The following sections will present the determination of the various parameters from the flight data, and where possible, they will also present analyses of the effects of Mach number and dynamic pressure.

Horizontal-Tail Lift Parameters

Sample time histories of information required for least-squares solutions of equations of the form of equation (17) for the coefficients Z, A', B', and C' are given in figures 3 and 4. The maneuver of figure 3 is a relatively fast push-pull, whereas the maneuver of

figure 4 is a slow pull-up from level flight (the only pull-up of the 68 maneuvers used in the present analysis). Both maneuvers were made at $M = 0.427$ and $q = 126$. In each figure the time histories of elevator angle δ_e, wing angle of attack α_w, and the measured tail aerodynamic tail load L_{T_A} are shown. Also included are the combined angle-of-attack parameters α_1 and α_2 defined by equations (19) and (20).

The determination of the coefficients of equation (17) by using least squares produced the following equations for the two sample maneuvers:

for data of figure 3 (flight 12, run 28),

$$L_{T_A} = 566 + 1963\alpha_1 - 949\alpha_2 + 874\delta_e \tag{31}$$

and for data of figure 4 (flight 11, run 24),

$$L_{T_A} = 66 + 1558\alpha_1 - 565\alpha_2 + 823\delta_e \tag{32}$$

The fit to the tail-load data for each run is indicated on figures 3 and 4 where tail loads calculated by use of equations (31) and (32) are shown in time-history form in comparison with the actual measured tail loads. The fit in both cases is seen to be excellent. Because both maneuvers were made at the same Mach number and dynamic pressure, more reliable values of the A', B', and C' coefficients were obtained when the two were considered together. Actual least-squares solution of the two maneuvers combined by using equations of the form of equation (18) produced the following numerical results:

for flight 11, run 24,

$$L_{T_A} = 1290 + 1971\alpha_1 - 976\alpha_2 + 883\delta_e \tag{33a}$$

for flight 12, run 28,

$$L_{T_A} = 740 + 1971\alpha_1 - 976\alpha_2 + 883\delta_e \tag{33b}$$

The standard error of fit for equations (33) was 109 pounds as compared with 69 pounds for flight 11, run 24 (eq. (32)) and 121 pounds for flight 12, run 28 (eq. (31)). The fit to the data for each run is also illustrated in figure 5 where the tail-load time histories calculated by equations (33) are compared with the measured tail loads. The agreement is still excellent.

Whenever possible the maneuvers with the same Mach number and dynamic pressure were combined for least-squares solutions. Where Mach number was relatively constant but dynamic pressure varied, the q-form (eq. (21)) was used for combination.

Variations of coefficients with Mach number and dynamic pressure.- The coefficients $C_{l_{\alpha_t}}$, $-\frac{d\epsilon}{d\alpha}C_{l_{\alpha_t}}$, and C_{l_δ} for the example maneuvers were obtained by correcting for fuselage bending due to tail load using equations of the form of equations (12) and (14) as

$$C_{l_{\alpha_t}} = \frac{A'}{1 + A'K_1}\frac{1}{qS_t} = \frac{1971}{1 - \frac{.578(1971)}{10^4}}\frac{1}{33768} = 0.0659$$

$$-\frac{d\epsilon}{d\alpha}C_{l_{\alpha_t}} = \frac{B'}{1 + A'K_1}\frac{1}{qS_t} = \frac{-976}{(.886)(33768)} = -0.0326$$

$$C_{l_\delta} = \frac{C'}{1 + A'K_1}\frac{1}{qS_t} = \frac{883}{29918} = 0.0295$$

The preceding coefficients are given in table III along with the coefficients computed from least-squares solutions of the remaining 66 maneuvers. The data in table III are grouped by altitude and in increasing Mach number order.

Values of $C_{l_{\alpha_t}}$ are plotted in figure 6(a) as a function of Mach number with different symbols to denote the altitude of the test point. No variation of $C_{l_{\alpha_t}}$ with dynamic pressure at constant Mach numbers could be established because of the small magnitude of the flexibility effect and the scatter of the data. Faired curves covering Mach number ranges above and below $M = 0.70$ were fitted to the data of figure 6(a) by least squares. Several forms of equations were tried, and equations containing Glauert type functions of Mach number and sweep angle were found to be applicable to the fairing of $C_{l_{\alpha_t}}$, C_{l_δ}, and $\frac{d\epsilon}{d\alpha}$. Since C_{l_δ} and $\frac{d\epsilon}{d\alpha}$ are not functions of the sweep angle of the horizontal-tail quarter-chord line, a nominal value of $\Lambda = 35^\circ$ was used for convenience for fairing all parameters.

The empirical equations determined as best representing the $C_{l_{\alpha_t}}$ data of figure 6(a) were

$$\left.\begin{aligned}\left(C_{l_{\alpha_t}}\right)_{M\leq.70} &= \frac{0.0596}{\sqrt{1 - M^2\cos^2\Lambda}} \\ \left(C_{l_{\alpha_t}}\right)_{M\geq.70} &= \frac{0.0400}{\left(\sqrt{1 - M^2\cos^2\Lambda}\right)^3}\end{aligned}\right\} \tag{34}$$

The variation of $C_{l_{\alpha_t}}$ with Mach number, as described by equations (34), is shown in figure 6(a) as the solid line.

The values of C_{l_δ} are plotted in figure 6(b) as a function of Mach number with different symbols to identify the altitudes of the tests. In this case a dynamic-pressure effect was evident, and least squaring of the coefficients produced the following empirical equations for the flight-test values of C_{l_δ}

$$\left.\begin{aligned}\left(C_{l_\delta}\right)_{M\leq.72} &= \frac{0.0303}{\sqrt{1 - M^2\cos^2\Lambda}}\left(1 - 0.1087\frac{q}{10^2}\right) \\ \left(C_{l_\delta}\right)_{M\geq.72} &= \frac{0.0244}{\left(\sqrt{1 - M^2\cos^2\Lambda}\right)^2}\left(1 - 0.1081\frac{q}{10^2}\right)\end{aligned}\right\} \tag{35}$$

The data in the Mach number ranges up to 0.72 and above 0.72 were least squared independently, and it may be noted that the dynamic pressure coefficients are almost identical. Calculated variations of C_{l_δ} (eqs. (35)) for the test altitudes and for $q = 0$ are also shown in figure 6(b). The flexibility effect as determined is believed to be due to bending and twisting of the elevator; however, the instrumentation was inadequate for a detailed analysis.

The values of the elevator effectiveness parameter $\frac{d\alpha_t}{d\delta_e}$ for each maneuver obtained by the use of equation (15) are given in table III and plotted in figure 7. The values of $\frac{d\alpha_t}{d\delta_e}$ obtained from faired values of C_{l_δ} and $C_{l_{\alpha_t}}$ by using equations (34) and (35) are also shown in figure 7 as a function of Mach number and altitude.

In order to determine the downwash parameter $\frac{d\epsilon}{d\alpha}$, the coefficient $-\frac{d\epsilon}{d\alpha}C_{l_{\alpha_t}}$ was plotted as a function of Mach number in figure 8. As in the case of $C_{l_{\alpha_t}}$ no definite effect of dynamic pressure could be established and the data were fitted by least squares with the empirical equations

$$\left.\begin{aligned}\left(-\frac{d\epsilon}{d\alpha}C_{l_{\alpha_t}}\right)_{M\leq.70} &= \frac{-0.0273}{\left(\sqrt{1 - M^2\cos^2\Lambda}\right)^2} \\ \left(-\frac{d\epsilon}{d\alpha}C_{l_{\alpha_t}}\right)_{M\geq.70} &= \frac{-0.0122}{\left(\sqrt{1 - M^2\cos^2\Lambda}\right)^6}\end{aligned}\right\} \tag{36}$$

The downwash parameters obtained from equation (13) are given in table III and plotted in figure 9 along with the empirical curve derived from the division of equations (36) by equations (34). The equations for $\frac{d\epsilon}{d\alpha}$ from this operation are

$$\left.\begin{aligned}\left(\frac{d\epsilon}{d\alpha}\right)_{M\leq.70} &= \frac{0.458}{\sqrt{1 - M^2\cos^2\Lambda}} \\ \left(\frac{d\epsilon}{d\alpha}\right)_{M\geq.70} &= \frac{0.305}{\left(\sqrt{1 - M^2\cos^2\Lambda}\right)^3}\end{aligned}\right\} \tag{37}$$

The coefficient for the low Mach number range of equation (37) indicates that from the present set of flight results for the test airplane the effective downwash factor $\frac{d\epsilon}{d\alpha}$ is 0.458 at $M = 0$.

Calculation of tail loads using faired coefficients.- As an overall check on the empirical equations (34), (35), and (36), for the tail-load parameters $C_{l_{\alpha_t}}$, $\frac{d\epsilon}{d\alpha}$, and $\frac{d\alpha_t}{d\delta_e}$ tail-load time histories were computed by using (1) least-squares coefficients from table III and (2) faired coefficients from equations (34), (35), and (36), and an adjusted zero shift Z' consistent with these coefficients. The adjusted zero shifts consistent with the faired values of $C_{l_{\alpha_t}}$, $-\frac{d\epsilon}{d\alpha}C_{l_{\alpha_t}}$, and C_{l_δ} were computed by rotating the data about the means of the variables α_1, α_2, and δ_e by the use of the equation

$$Z' = Z - qS_t\left[\left(C_{l_{\alpha_t}}\right)_f - \left(C_{l_{\alpha_t}}\right)_m\right]\bar{\alpha}_1 - qS_t\left[\left(-\frac{d\epsilon}{d\alpha}C_{l_{\alpha_t}}\right)_f - \left(-\frac{d\epsilon}{d\alpha}C_{l_{\alpha_t}}\right)_m\right]\bar{\alpha}_2 - qS_t\left[\left(C_{l_\delta}\right)_f - \left(C_{l_\delta}\right)_m\right]\bar{\delta}_e \quad (38)$$

The subscripts f and m in equation (38) refer to faired and measured values of the coefficients; the bar over α_1, α_2, and δ_e indicates mean values for the particular maneuver being considered. The results of the calcualtion of Z' from equation (38) are given in the last column of table III and represent the best estimate of the zero shift for each maneuver. The largest difference between values of Z and Z' is approximately 1,400 pounds.

Sample calculations of tail-load time histories made by using measured coefficients with measured zero shifts and faired coefficients with faired zero shifts are given for a maneuver (flight 10, run 7) where considerable differences appeared to exist between the individual run coefficients and the faired values. Equations (11) to (14) and the data of table III provide the least-squares coefficients for recalculating a tail-load time history as the following equations:

for flight 10, run 7,

$$L_{T_A} = 5830 + \frac{0.0752qS_t(\alpha_1)}{1 + \frac{.578(.0752)qS_t}{10^4}} - \frac{0.0441qS_t(\alpha_2)}{1 + \frac{.578(.0752)qS_t}{10^4}} + \frac{0.0283qS_t\delta_e}{1 + \frac{.578(.0752)qS_t}{10^4}}$$

or with

$$qS_t = 68{,}072 \text{ lb}$$

$$L_{T_A} = 5830 + 3950\alpha_1 - 2316\alpha_2 + 1486\delta_e \quad (39)$$

Using the faired coefficients for the same run and the rotated zero shift from table III the following equation is obtained for the same maneuver (flight 10, run 7):

$$L_{T_A} = 6990 + 4306\alpha_1 - 2760\alpha_2 + 1483\delta_e \quad (40)$$

The differences between equation (39) (the tail load calculated from least-squares coefficients) and equation (40) (the tail load calculated from faired coefficients) are shown graphically in figure 10 where the two calculated load time histories are compared with the measured tail loads. The fit to the measured data is good in both cases, the root-mean-square error being 54 pounds for equation (39) and 107 pounds for equation (40).

Centers of Pressure

As explained in the section entitled "Methods" of the present paper, the centers of pressure of the loads due to angle of attack, downwash, and elevator deflection were obtained from equations (25) and (26). The spanwise and chordwise centers of pressure for maneuvers selected to cover the Mach number and dynamic-pressure range of the data are given in table IV. Attempts to ascertain Mach number or dynamic-pressure effects were unsuccessful because of the scatter of the results. Consequently, the envelopes of the centers of pressure are plotted in figure 11 which is a diagram of a half tail of the test airplane showing the 0.25c line, the 0.50c line, the strain-gage reference station, and the elevator hinge line, the 0.70c line. The mean chord of the area outboard of the strain-gage station is also indicated. The envelope of the α_1 loads is seen to be within the envelope of the α_2 or downwash loads and near the intersection of the mean-chord line and the quarter-chord line. The envelope of the elevator-load centers of pressure is somewhat outboard of the α_1 and α_2 locations. The mean values of the center-of-pressure locations from table IV in terms of the percent semispan outboard of the gage station and percent mean chord at the spanwise center of pressure are listed below along with the standard errors.

Loading	Spanwise c.p., percent semispan outboard of strain-gage station	Standard error of spanwise c.p., percent	Chordwise c.p., percent local chord at spanwise c.p. location	Standard error of chordwise c.p., percent
α_1	48.6	±1.5	18.1	±1.6
α_2	48.8	±2.8	19.0	±2.8
δ_e	51.2	±1.5	45.3	±2.7

For the maneuvers (flight 11, run 24 and flight 12, run 28) the probable errors in the centers of pressure determined from the least-squares equations are given in table IV. These probable errors are approximately the same size as the errors for the average centers of pressure given in the preceding table and indicate, as stated previously, that scatter of the data probably masked any real Mach number or dynamic-pressure effects on center-of-pressure location.

Tail Pitching-Moment Coefficient Due to Elevator Deflection

The tail pitching-moment coefficient about the 25-percent-chord location of the tail mean aerodynamic chord was obtained by the use of equation (30) with values of C_T and x_δ from least-squares solutions for individual or combined maneuvers. The values of $C_{m_{\delta_t}}$ per radian for all 68 maneuvers are plotted in figure 12 as a function of Mach number. The data points are distinguished for altitudes of 20,000, 25,000, 30,000, and 35,000 feet. There is a tendency for the lower altitude data to have smaller values of $C_{m_{\delta_t}}$. The variation of C_{l_δ} with dynamic pressure and the expected effects of elevator flexibility are in agreement with this trend, but a detailed analysis did not appear to be warranted.

Comparisons

Horizontal-tail lift parameters.- Wind-tunnel data on plan forms of the same aspect ratio, taper ratio, and sweep angle as those for the horizontal tail of the test airplane are very limited. An investigation of a full-scale empennage of the test airplane at low speeds is reported in reference 4. From page 53 of reference 4, the parameters $C_{l_{\alpha_t}}$, C_{l_δ}, and $\frac{d\alpha_t}{d\delta_e}$ were determined for the full-scale tunnel-test condition of $q = 28.9$ pounds per square foot. The results of this evaluation are given in the following table and compared with the zero Mach number constants of equations (34) and (35).

	$C_{l_{\alpha_t}}$	C_{l_δ}	$\frac{d\alpha_t}{d\delta_e}$
Flight-test equations (34) and (35)	0.0595	0.0303	0.508
Full-scale tunnel test, ref. 4	0.0583	0.0305	0.523

The agreement between the flight-test and wind-tunnel values is excellent in this case.

In reference 4, the downwash parameter $\frac{d\epsilon}{d\alpha}$ was determined from wind-tunnel pitching-moment-coefficient measurements ($M = 0.30$) as being equal to 0.31. The flight-test values of the downwash parameter, equation (37), at a Mach number of zero is 0.458. The disagreement may be due to the necessary use in reference 4 of two different sets of wind-tunnel data in order to estimate the downwash factor.

Centers of pressure and tail pitching-moment coefficient due to elevator angle.- No wind-tunnel center-of-pressure measurements exist for direct comparison with the flight-test values; however, it is evident from figure 11 that the spanwise and chordwise centers of pressure of the α_1 and α_2 loads are reasonably close to lifting-line-theory locations. The chordwise center of pressure of the load due to elevator deflection is naturally a function of section $C_{m_{\delta_t}}$ for which there are data available from section pressure distributions obtained at the 1/3 and 2/3 semispan stations and reported in reference 5. The following table gives a comparison of section $C_{m_{\delta_t}}$ about the section quarter chord and $C_{m_{\delta_t}}$ for the complete tail from the low Mach number flight-test values shown in figure 12.

Source	Section $c_{m_{\delta_c/4}}$, per radian	$C_{m_{\delta_t}}$ for complete tail, per radian
Flight test (fig. 12), $M \approx 0.42$	-----	-0.50
Ref. 5 ($\frac{1}{3}$ - semispan location)	-0.49	-----
Ref. 5 ($\frac{2}{3}$ - semispan location)	-0.45	-----

The agreement indicated in the preceding table is good, and thus the centers of pressure computed by using theoretical methods would be in essential agreement with the flight-test values.

CONCLUDING REMARKS

Horizontal-tail loads measured by means of strain gages mounted at the root of the horizontal tail of a large flexible swept-wing jet bomber have been used to determine tail-load parameters useful in the calculation of airplane static and dynamic stability characteristics. The methods used were essentially least-squares curve-fitting techniques and allowed for fuselage bending under both inertia load and

aerodynamic tail load. The determination of the tail lift-curve slope due to tail angle of attack $C_{l_{\alpha_t}}$, tail lift-curve slope due to elevator deflection C_{l_δ}, downwash factor $\frac{d\epsilon}{d\alpha}$, and the elevator effectiveness factor $\frac{d\alpha_t}{d\delta_e}$ by the methods of this report should be generally applicable to flight-test tail-load data, providing accurate angle-of-attack measurements are available and pitching maneuvers are used which are abrupt enough to permit the separation of the unknown variables by least-squares procedures. A method of determining zero shifts in measured tail loads, useful when absolute values of tail load are desired, is also given.

Specifically for the test airplane it was found that:

1. The effect of horizontal-stabilizer flexibility on the tail lift-curve slope could not be determined, presumably because of the scatter of the data and the small magnitude of the flexibility effect.

2. The effects of elevator flexibility were readily determinable and were found to be approximately linear with dynamic pressure over the complete Mach number range.

3. No effect of wing flexibility on the downwash factor $\frac{d\epsilon}{d\alpha}$ could be found, probably because of the fact that the wing forward of the tail is relatively rigid.

Direct comparisons, where possible, between flight and low-speed wind-tunnel results for the $C_{l_{\alpha_t}}$, C_{l_δ}, $\frac{d\alpha_t}{d\delta_e}$, and tail pitching-moment coefficient due to elevator deflection $C_{m_{\delta_t}}$, and centers of pressure indicated almost exact agreement. The disagreement between values of $\frac{d\epsilon}{d\alpha}$ measured in flight and values of $\frac{d\epsilon}{d\alpha}$ determined by analysis of wind-tunnel data was large. At a Mach number of 0.30 wind-tunnel data indicated that the downwash factor $\frac{d\epsilon}{d\alpha}$ was equal to 0.31, whereas the flight test value of $\frac{d\epsilon}{d\alpha}$ at this Mach number was found to be 0.47. Although no wind-tunnel test values are available up to the maximum Mach number of the present tests ($M = 0.81$) it is believed that the flight results reported herein are accurate over the complete Mach

number range and may be used for stability calculations with the inclusion of dynamic response terms in the equations of motion when necessary.

Langley Aeronautical Laboratory,
National Advisory Committee for Aeronautics,
Langley Field, Va., September 21, 1956.

REFERENCES

1. Aiken, William S., Jr., and Wiener, Bernard: Analysis of the Horizontal-Tail Loads Measured in Flight on a Multiengine Jet Bomber. NACA TN 3479, 1955.

2. Aiken, Wiliam S., Jr., and Fisher, Raymond A.: Lift-Curve Slopes Determined in Flight on a Flexible Swept-Wing Jet Bomber. NACA RM L56E21a, 1956.

3. Skopinski, T. H., Aiken, William S., Jr., and Huston, Wilber B.: Calibration of Strain-Gage Installations in Aircraft Structures for the Measurement of Flight Loads. NACA Rep. 1178, 1954. (Supersedes NACA TN 2993.)

4. Ganzer, V. M., and Sandoz, Paul: Full Scale Test of the XB-47 Empennage. Part I - Analysis and Force Data. Doc. No. D-8517, Boeing Airplane Co., Aug. 5, 1947.

5. Brown, R. B., and Perkins, Grace: Full Scale Test of the XB-47 Empennage. Part II - Pressure Data. Doc. No. D-8517-1, Boeing Airplane Co., Oct. 27, 1948.

TABLE I.- AIRPLANE CHARACTERISTICS AND DIMENSIONS

Horizontal Tail:	
Total area, sq ft	268
Span, ft	33
Root chord, ft	11.42
Mean aerodynamic chord, ft	8.58
Distance from horizontal tail 0.25 M.A.C. to wing 0.25 M.A.C., ft	46.52
Incidence angle, deg	-0.25
Sweepback (25-percent-chord line), deg	32.9
Aspect ratio	4.06
Taper ratio	0.423
Airfoil section	BAC 100
Strain-gage reference station (percent semispan)	5.3
Wing:	
Total area, sq ft	1428
Span, ft	116
Mean aerodynamic chord, ft	13
Aspect ratio	9.42
Taper ratio	0.420
Incidence angle, deg	2.75
Sweepback (25-percent-chord line), deg	35
Airfoil section	BAC 145

TABLE II.- SUMMARY OF FLIGHT CONDITIONS

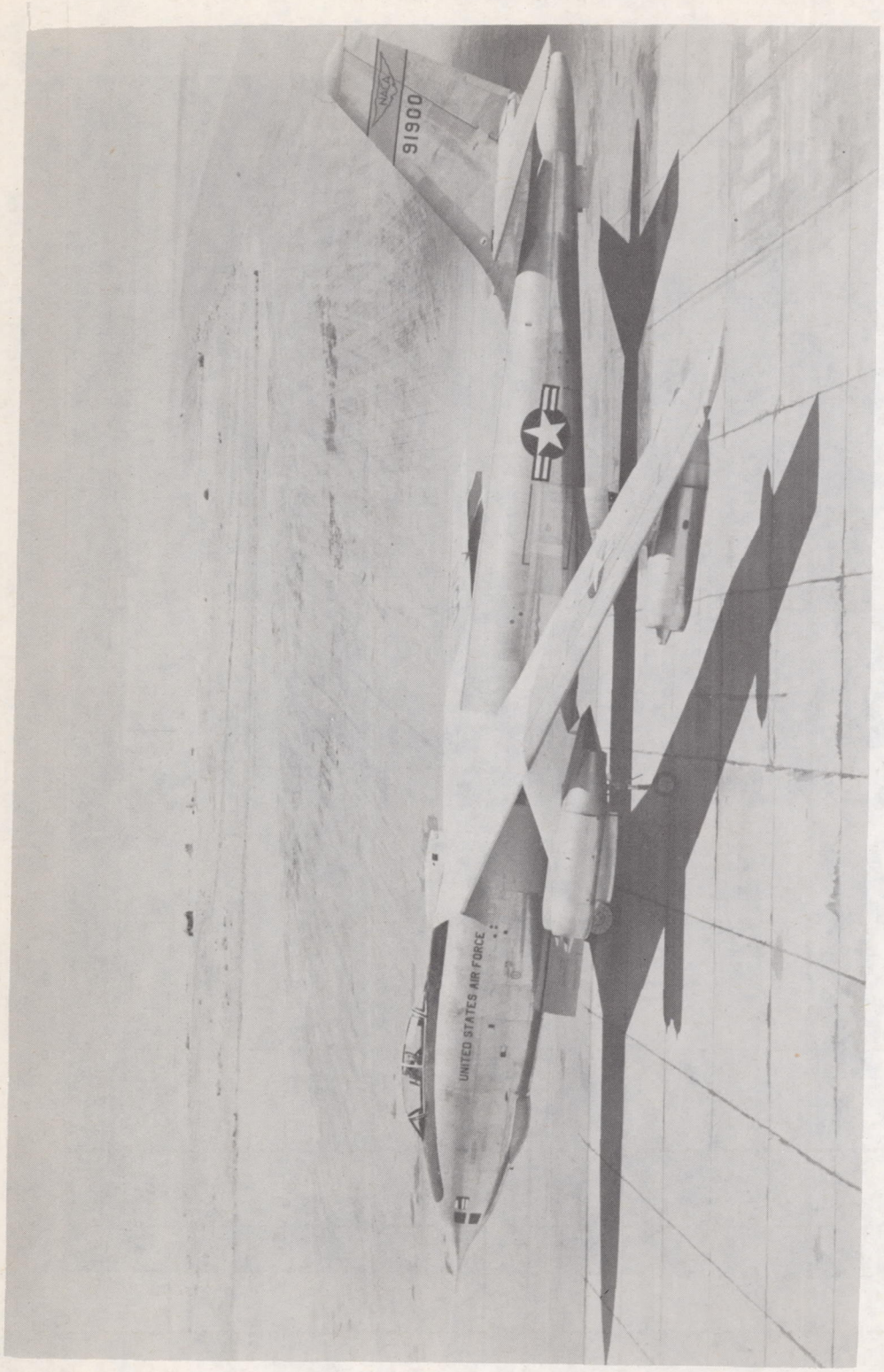
Flight	Run	M_{av}	q_{av}, lb/sq ft	Pressure altitude, ft	W, lb	Center-of-gravity location, percent M.A.C.
2	27	0.636 ± 0.002	137 ± 2	35,200	112,600	21.1
	28	0.735 ± 0.001	184 ± 1	34,900	112,300	21.3
	29	0.796 ± 0.004	216 ± 2	34,800	112,200	21.5
3	11	0.750 ± 0.001	196 ± 1	34,600	120,300	13.6
	12	0.728 ± 0.007	188 ± 5	34,100	120,100	13.6
	13	0.689 ± 0.006	167 ± 3	34,400	119,900	13.5
	14	0.631 ± 0.002	140 ± 1	34,600	119,000	13.4
4	19	0.699 ± 0.002	264 ± 3	25,000	108,900	21.0
	20	0.591 ± 0.001	190 ± 1	25,000	108,700	20.9
	21	0.486 ± 0.003	128 ± 1	25,300	108,400	20.8
6	11	0.789 ± 0.001	264 ± 3	30,800	108,800	13.1
	12	0.790 ± 0.001	268 ± 1	30,500	108,700	13.1
	13	0.741 ± 0.001	244 ± 1	29,800	108,400	13.1
	14	0.690 ± 0.001	215 ± 1	29,400	108,200	13.2
	15	0.643 ± 0.003	187 ± 2	29,400	107,600	13.0
8	4	0.544 ± 0.008	163 ± 4	24,900	124,800	22.6
	5	0.648 ± 0.004	233 ± 3	24,800	124,500	22.8
	6	0.758 ± 0.002	314 ± 4	25,100	124,000	23.2
9	1	0.598 ± 0.003	125 ± 1	34,800	126,700	22.6
	2	0.647 ± 0.004	147 ± 2	34,900	126,200	22.5
	3	0.681 ± 0.001	161 ± 1	35,200	126,100	22.7
	4	0.731 ± 0.003	185 ± 1	35,200	125,700	22.9
	5	0.779 ± 0.002	214 ± 1	34,900	125,400	23.1
	6	0.795 ± 0.001	216 ± 1	35,500	125,200	23.3
	7	0.810 ± 0	225 ± 1	35,300	124,900	23.5
10	3	0.598 ± 0.003	159 ± 2	29,800	127,200	22.6
	4	0.647 ± 0.001	185 ± 0	29,900	126,500	22.3
	5	0.681 ± 0.001	200 ± 1	30,500	126,300	22.4
	6	0.726 ± 0.001	230 ± 1	30,200	126,100	22.5
	7	0.763 ± 0	254 ± 0	30,200	125,400	23.0
	8	0.789 ± 0	260 ± 1	31,100	125,200	23.1
	9	0.812 ± 0.001	274 ± 1	31,300	124,900	23.3
11	11	0.495 ± 0.003	138 ± 1	24,400	109,200	21.8
	12	0.542 ± 0.003	164 ± 1	24,600	108,900	21.7
	13	0.597 ± 0.001	194 ± 1	25,100	108,500	21.8
	14	0.636 ± 0	222 ± 0	25,000	108,500	21.8
	15	0.681 ± 0	247 ± 0	25,700	108,400	21.9
	16	0.702 ± 0.001	266 ± 1	25,400	107,800	21.7
	17	0.734 ± 0	291 ± 0	25,300	107,500	21.8
	24	0.427 ± 0.001	126 ± 1	19,700	103,700	22.2
12	6	0.584 ± 0.001	127 ± 1	33,700	120,400	14.5
	7	0.642 ± 0.001	147 ± 1	34,400	120,300	14.6
	8	0.679 ± 0.001	162 ± 0	34,900	119,900	14.6
	9	0.721 ± 0.001	178 ± 1	35,300	119,600	14.6
	10	0.773 ± 0.001	202 ± 1	35,400	119,100	14.7
	11	0.790 ± 0	215 ± 0	35,200	118,800	14.6
	12	0.812 ± 0	228 ± 0	35,200	118,700	14.4
	17	0.483 ± 0.001	130 ± 1	24,600	116,600	13.8
	18	0.532 ± 0	157 ± 0	24,700	116,500	13.7
	19	0.600 ± 0.001	198 ± 1	24,900	116,400	13.7
	20	0.637 ± 0	223 ± 0	25,000	116,300	13.8
	21	0.682 ± 0.001	255 ± 1	25,000	116,100	13.9
	22	0.694 ± 0.001	262 ± 0	25,200	115,800	14.1
	23	0.735 ± 0.001	298 ± 1	24,900	115,400	14.3
	24	0.642 ± 0.002	279 ± 3	20,000	111,100	21.5
	25	0.595 ± 0.002	242 ± 1	19,800	111,100	21.5
	26	0.543 ± 0	202 ± 1	19,700	110,600	21.6
	27	0.482 ± 0.002	159 ± 1	19,700	110,300	21.9
	28	0.427 ± 0.001	126 ± 1	19,600	110,200	21.6
16	1	0.642 ± 0.001	282 ± 1	19,900	117,100	14.6
	2	0.599 ± 0.002	246 ± 2	19,800	116,800	14.3
	3	0.542 ± 0.002	200 ± 2	20,000	116,600	13.6
	4	0.482 ± 0.002	160 ± 1	19,800	116,000	13.9
	5	0.428 ± 0.003	127 ± 2	19,500	115,500	13.7
	6	0.433 ± 0.002	131 ± 2	19,300	115,100	13.5
17	5	0.808 ± 0.001	364 ± 1	24,600	116,400	14.2
	6	0.762 ± 0	326 ± 0	24,500	116,200	14.2
	7	0.725 ± 0	295 ± 0	24,500	115,600	14.0

TABLE III.- HORIZONTAL-TAIL PARAMETERS FROM LEAST-SQUARES ANALYSES

Approximate altitude, ft	Flight	Run	M_{av}	$C_{l_{\alpha_t}}$, per deg	C_{l_δ}, per deg	$-\frac{d\epsilon}{d\alpha}C_{l_{\alpha_t}}$, per deg	$\frac{d\epsilon}{d\alpha}$	$\frac{d\alpha_t}{d\delta_e}$	Z, lb	Z', lb
20,000	11	24	0.427	0.0659	0.0295	-0.0326	0.495	0.448	1,290	1,000
	12	28	.427	.0659	.0295	-.0326	.495	.448	740	560
	16	5	.428	.0712	.0307	-.0387	.543	.431	5,630	4,570
	16	6	.433	.0690	.0297	-.0375	.543	.430	4,990	4,090
	12	27	.482	.0648	.0282	-.0316	.488	.435	-70	20
	16	4	.482	.0644	.0280	-.0314	.488	.435	4,950	4,980
	16	3	.542	.0646	.0271	-.0315	.487	.420	5,330	5,590
	12	26	.543	.0639	.0268	-.0311	.487	.419	-750	-360
	12	25	.595	.0686	.0262	-.0363	.529	.382	-1,460	-1,530
	16	2	.599	.0689	.0263	-.0364	.529	.382	6,210	6,080
	12	24	.642	.0685	.0263	-.0361	.527	.384	-2,450	-2,080
	16	1	.642	.0677	.0260	-.0357	.527	.384	5,960	6,190
25,000	12	17	.483	.0628	.0282	-.0288	.458	.449	-3,230	-2,720
	4	21	.486	.0627	.0282	-.0287	.458	.450	300	740
	11	11	.495	.0634	.0285	-.0290	.458	.450	1,100	1,540
	12	18	.532	.0657	.0284	-.0329	.501	.432	-2,990	-2,880
	11	12	.542	.0662	.0285	-.0332	.502	.431	1,110	1,210
	8	4	.544	.0660	.0285	-.0331	.502	.432	10,460	10,530
	4	20	.591	.0628	.0260	-.0300	.478	.414	-1,160	-370
	11	13	.597	.0630	.0260	-.0301	.477	.413	580	1,280
	12	19	.600	.0633	.0261	-.0303	.478	.412	-4,430	-3,460
	11	14	.636	.0675	.0263	-.0347	.514	.390	-500	-100
	12	20	.637	.0672	.0262	-.0345	.514	.390	-4,570	-4,050
	8	5	.648	.0646	.0264	-.0327	.506	.409	8,110	9,440
	11	15	.681	.0707	.0264	-.0392	.554	.373	-510	-450
	12	21	.682	.0713	.0267	-.0395	.554	.374	-4,670	-4,640
	12	22	.694	.0716	.0264	-.0390	.545	.369	-4,370	-4,150
	4	19	.699	.0711	.0262	-.0386	.543	.368	-1,380	-1,060
	11	16	.702	.0707	.0261	-.0383	.542	.369	-1,270	-890
	17	7	.725	.0738	.0254	-.0423	.573	.344	3,700	4,080
	11	17	.734	.0783	.0260	-.0459	.586	.332	-820	-700
	12	23	.735	.0789	.0263	-.0462	.586	.333	-3,740	-3,590
	8	6	.758	.0744	.0257	-.0443	.595	.345	8,070	9,140
	17	6	.762	.0754	.0261	-.0448	.594	.346	3,170	4,550
	17	5	.808	.0909	.0250	-.0646	.711	.275	4,280	4,890
30,000	10	3	.598	.0685	.0275	-.0378	.552	.401	13,970	13,720
	6	15	.643	.0683	.0275	-.0358	.524	.403	1,460	1,780
	10	4	.647	.0666	.0278	-.0359	.524	.405	11,200	11,430
	10	5	.681	.0721	.0280	-.0412	.572	.388	10,290	10,040
	6	14	.690	.0735	.0285	-.0419	.570	.388	2,230	1,940
	10	6	.726	.0779	.0282	-.0465	.597	.362	8,070	7,910
	6	13	.741	.0795	.0287	-.0471	.592	.361	2,320	2,510
	10	7	.763	.0752	.0283	-.0441	.586	.376	5,830	6,990
	6	11	.789	.0854	.0284	-.0565	.662	.333	2,640	3,350
	10	8	.789	.0867	.0288	-.0574	.662	.332	5,700	6,190
	6	12	.790	.0841	.0279	-.0557	.662	.332	2,370	3,280
	10	9	.812	.0968	.0298	-.0714	.738	.308	7,230	7,070
35,000	12	6	.584	.0742	.0301	-.0423	.570	.406	9,530	8,950
	9	1	.598	.0751	.0306	-.0428	.570	.414	16,450	16,080
	3	14	.631	.0723	.0282	-.0403	.557	.390	3,340	3,230
	2	27	.636	.0731	.0288	-.0407	.557	.394	1,210	1,010
	12	7	.642	.0757	.0295	-.0446	.589	.390	9,060	8,500
	9	2	.647	.0757	.0295	-.0446	.589	.390	15,190	14,630
	12	8	.679	.0736	.0287	-.0422	.574	.390	7,300	7,200
	9	3	.681	.0734	.0288	-.0423	.576	.392	12,670	12,420
	3	13	.689	.0740	.0290	-.0426	.575	.392	3,060	2,900
	12	9	.721	.0773	.0300	-.0448	.580	.388	6,070	6,070
	3	12	.728	.0784	.0303	-.0452	.577	.386	2,750	2,840
	9	4	.731	.0811	.0316	-.0502	.619	.390	12,190	11,750
	2	28	.735	.0816	.0318	-.0503	.617	.390	530	120
	3	11	.750	.0788	.0292	-.0474	.602	.371	2,980	3,460
	12	10	.773	.0912	.0310	-.0634	.695	.340	6,090	5,440
	9	5	.779	.0927	.0315	-.0645	.696	.340	10,410	9,830
	12	11	.790	.0918	.0322	-.0632	.688	.351	5,360	5,290
	9	6	.795	.0913	.0320	-.0629	.689	.350	8,650	8,810
	2	29	.796	.0915	.0320	-.0628	.686	.350	190	430
	9	7	.810	.1070	.0342	-.0808	.755	.320	9,540	8,660
	12	12	.812	.1057	.0337	-.0798	.755	.319	5,330	4,310

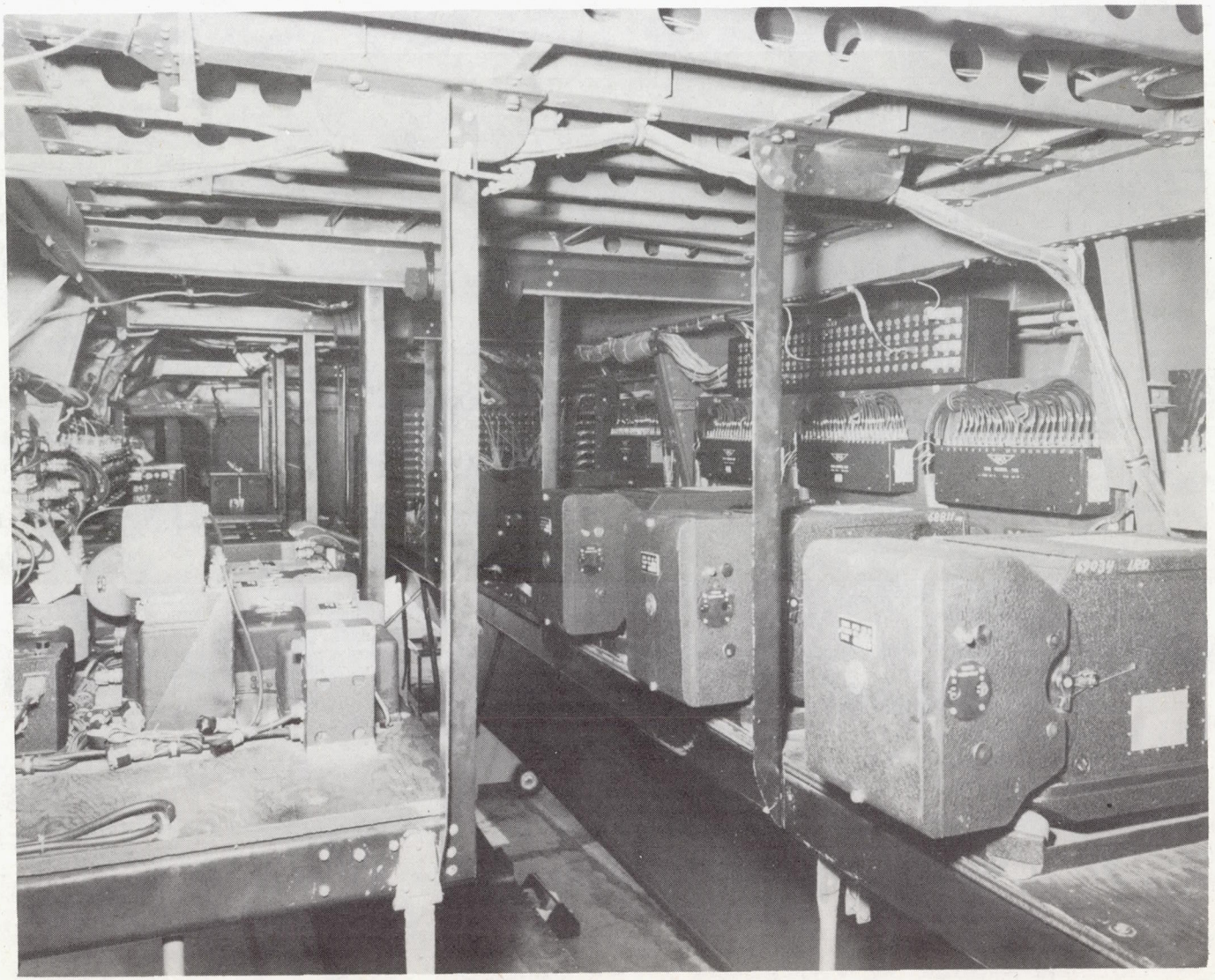
TABLE IV.- HORIZONTAL-TAIL CENTER-OF-PRESSURE LOCATIONS

Flight	Run	M_{av}	q_{av}, lb/sq ft	y_δ, in.	x_δ, in.	y_{α_1}, in.	x_{α_1}, in.	y_{α_2}, in.	x_{α_2}, in.
11	24	0.427	126	88.1 ± 0.8	-40.0 ± 0.4	83.4 ± 1.3	-14.8 ± 0.5	80.1 ± 3.5	-12.2 ± 1.4
12	28			88.1 ± 0.8	-40.0 ± 0.4	83.4 ± 1.3	-14.8 ± 0.5	80.1 ± 3.5	-12.2 ± 1.4
12	27	.482	159	90.2	-42.0	86.9	-15.7	88.8	-16.7
16	4			90.2	-42.0	86.9	-15.7	88.8	-16.7
9	1	.590	126	86.9	-40.8	86.0	-15.7	86.8	-15.6
12	6			86.9	-40.8	86.0	-15.7	86.8	-15.6
4	20	.596	194	93.9	-43.2	89.4	-15.0	92.9	-16.0
11	13			93.9	-43.2	89.4	-15.0	92.9	-16.0
12	19			93.9	-43.2	89.4	-15.0	92.9	-16.0
12	25	.597	244	92.3	-44.1	88.0	-16.6	87.4	-18.4
16	2			92.3	-44.1	88.0	-16.6	87.4	-18.4
10	3	.599	159	86.6	-46.4	82.8	-19.6	81.3	-23.0
10	4	.645	186	89.6	-45.5	84.0	-17.8	84.0	-19.7
6	15			89.6	-45.5	84.0	-17.8	84.0	-19.7
11	15	.682	251	94.1	-44.7	90.3	-14.8	94.2	-15.4
12	21			94.1	-44.7	90.3	-14.8	94.2	-15.4
12	8	.682	163	89.3	-44.0	86.3	-16.1	87.7	-16.4
9	3			89.3	-44.0	86.3	-16.1	87.7	-16.4
3	13			89.3	-44.0	86.3	-16.1	87.7	-16.4
10	5	.685	206	87.5	-45.7	85.3	-18.3	86.1	-20.7
6	14			87.5	-45.7	85.3	-18.3	86.1	-20.7
6	13	.733	237	90.4	-47.0	85.4	-18.5	85.9	-20.9
10	6			90.4	-47.0	85.4	-18.5	85.9	-20.9
10	8	.789	264	89.9	-49.1	82.1	-17.6	78.3	-18.3
6	11			89.9	-49.1	82.1	-17.6	78.3	-18.3
6	12			89.9	-49.1	82.1	-17.6	78.3	-18.3
2	29	.794	216	92.8	-45.6	87.6	-15.4	88.7	-14.8
9	6			92.8	-45.6	87.6	-15.4	88.7	-14.8
12	11			92.8	-45.6	87.6	-15.4	88.7	-14.8
17	5	.808	340	95.9	-49.4	83.0	-14.0	77.8	-13.0
9	7	.811	226	95.4	-46.4	89.4	-18.0	91.4	-18.6
12	12			95.4	-46.4	89.4	-18.0	91.4	-18.6
10	9	.812	274	91.6	-50.8	85.0	-18.5	84.1	-18.3



L-86692

Figure 1.- Side view of test airplane.



L-95849

Figure 2.- Recording instrumentation mounted in bomb bay of test airplane.

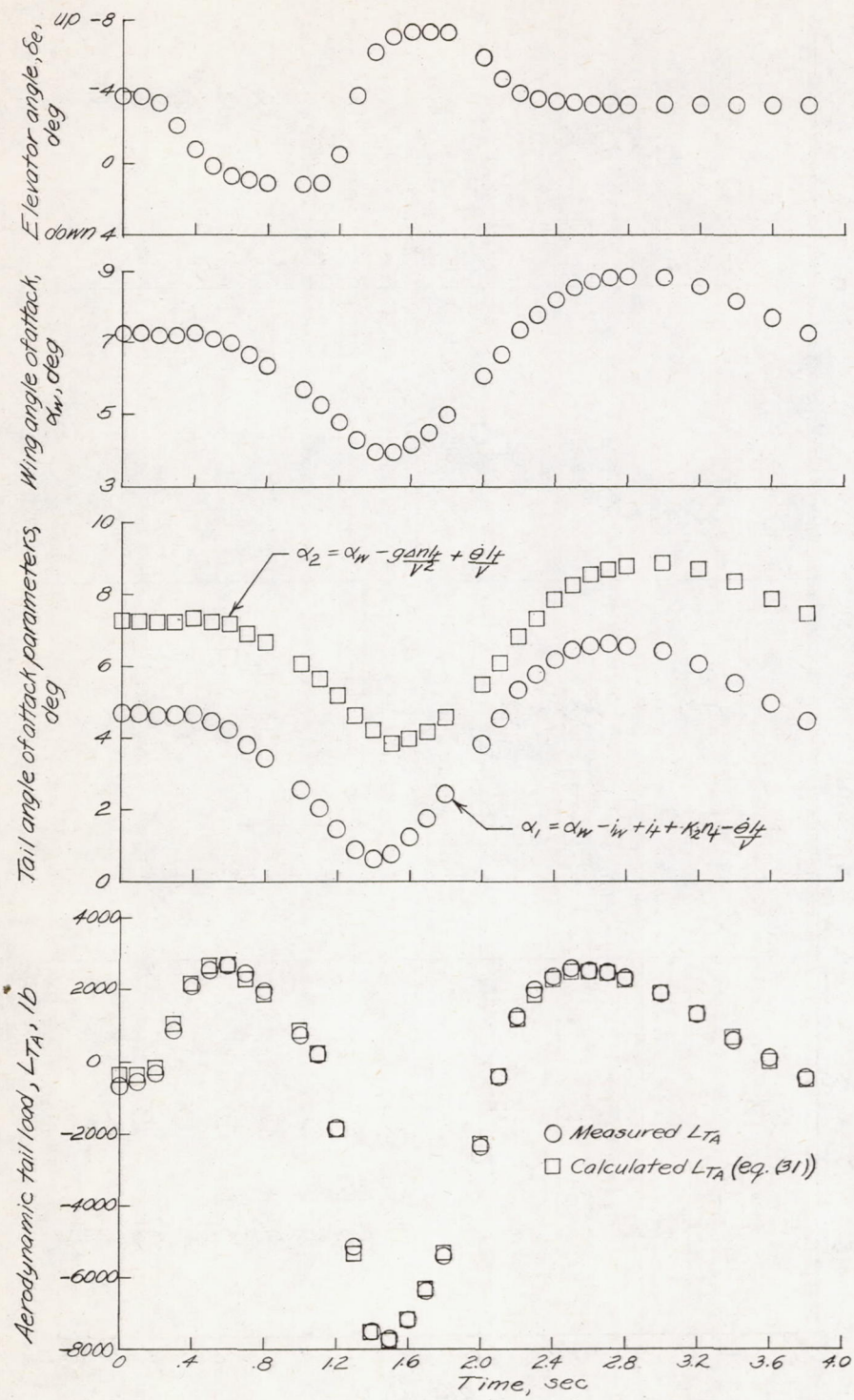


Figure 3.- Time histories for push-pull maneuver. Flight 12, run 28.

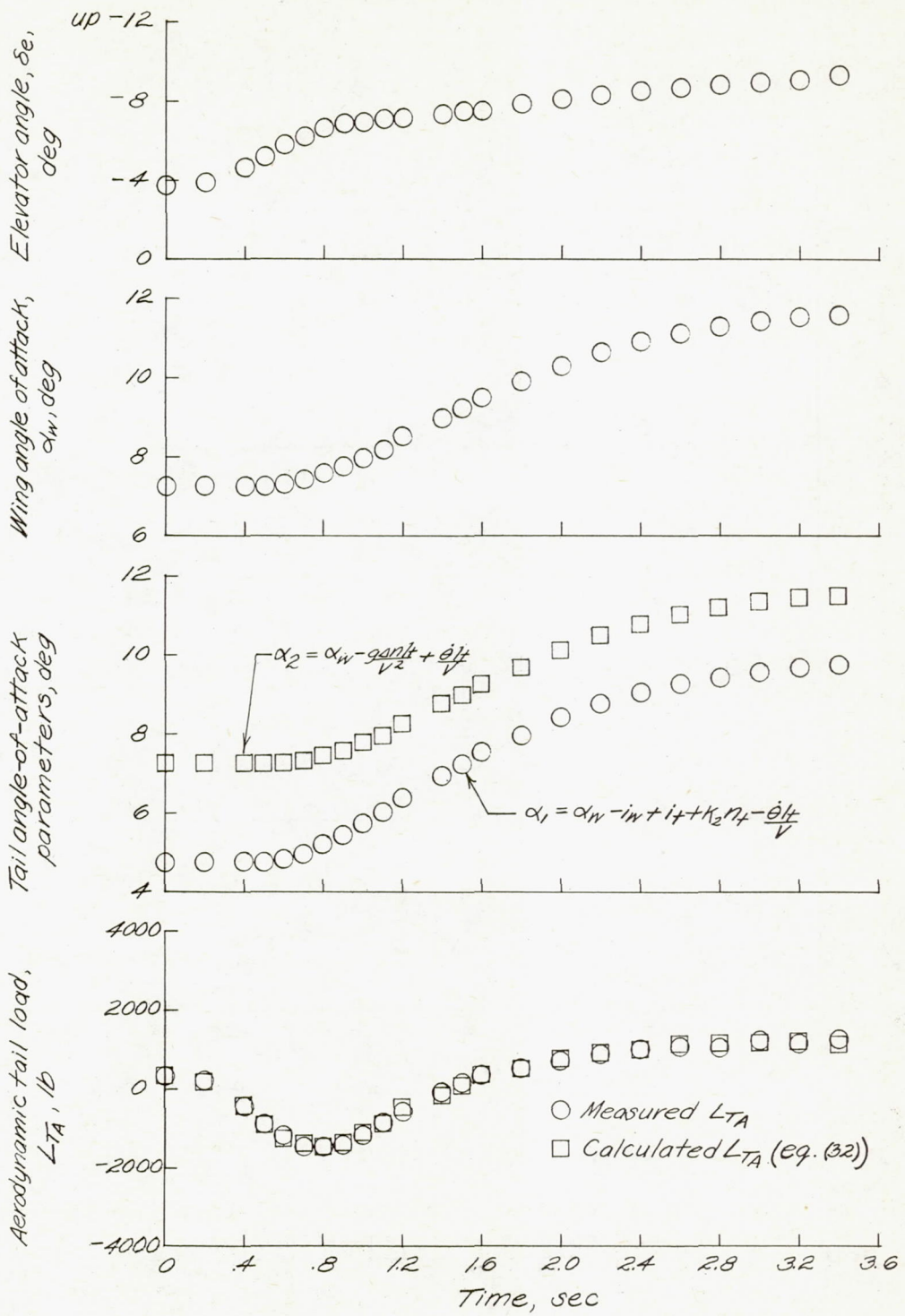
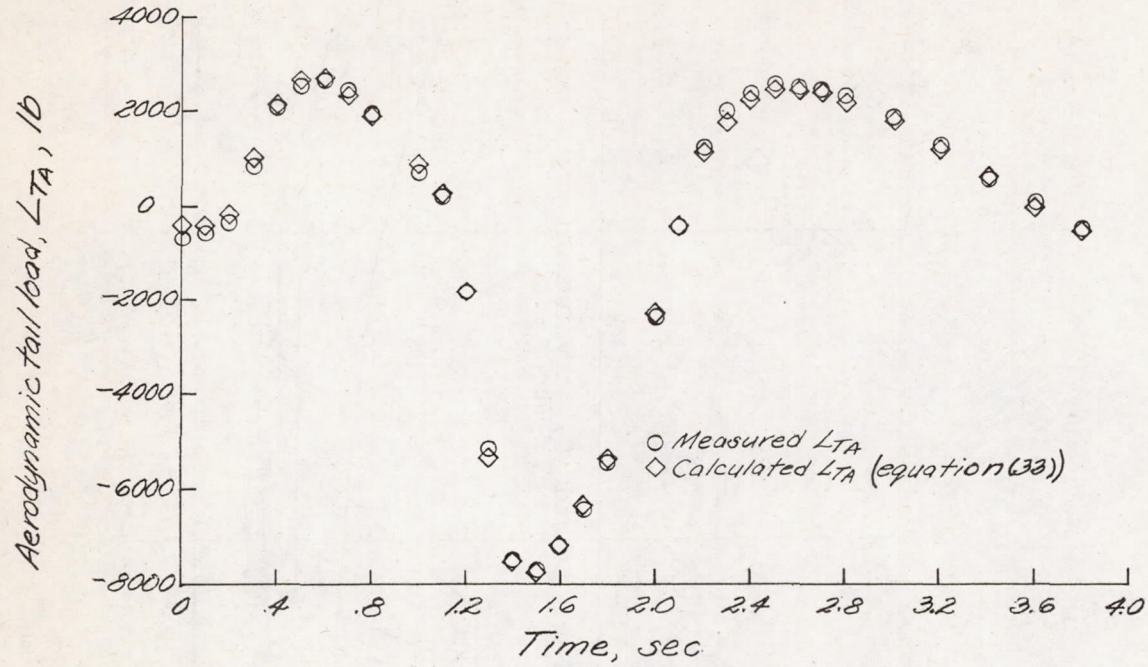
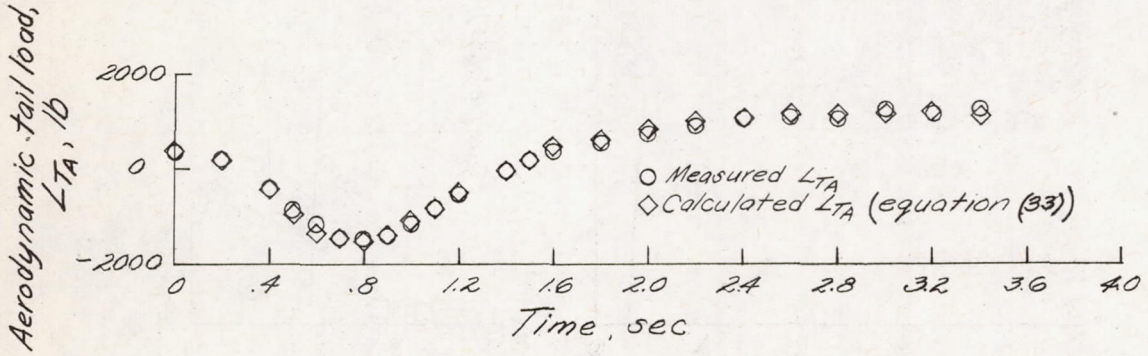


Figure 4.- Time histories for pull-up maneuver. Flight 11, run 24.

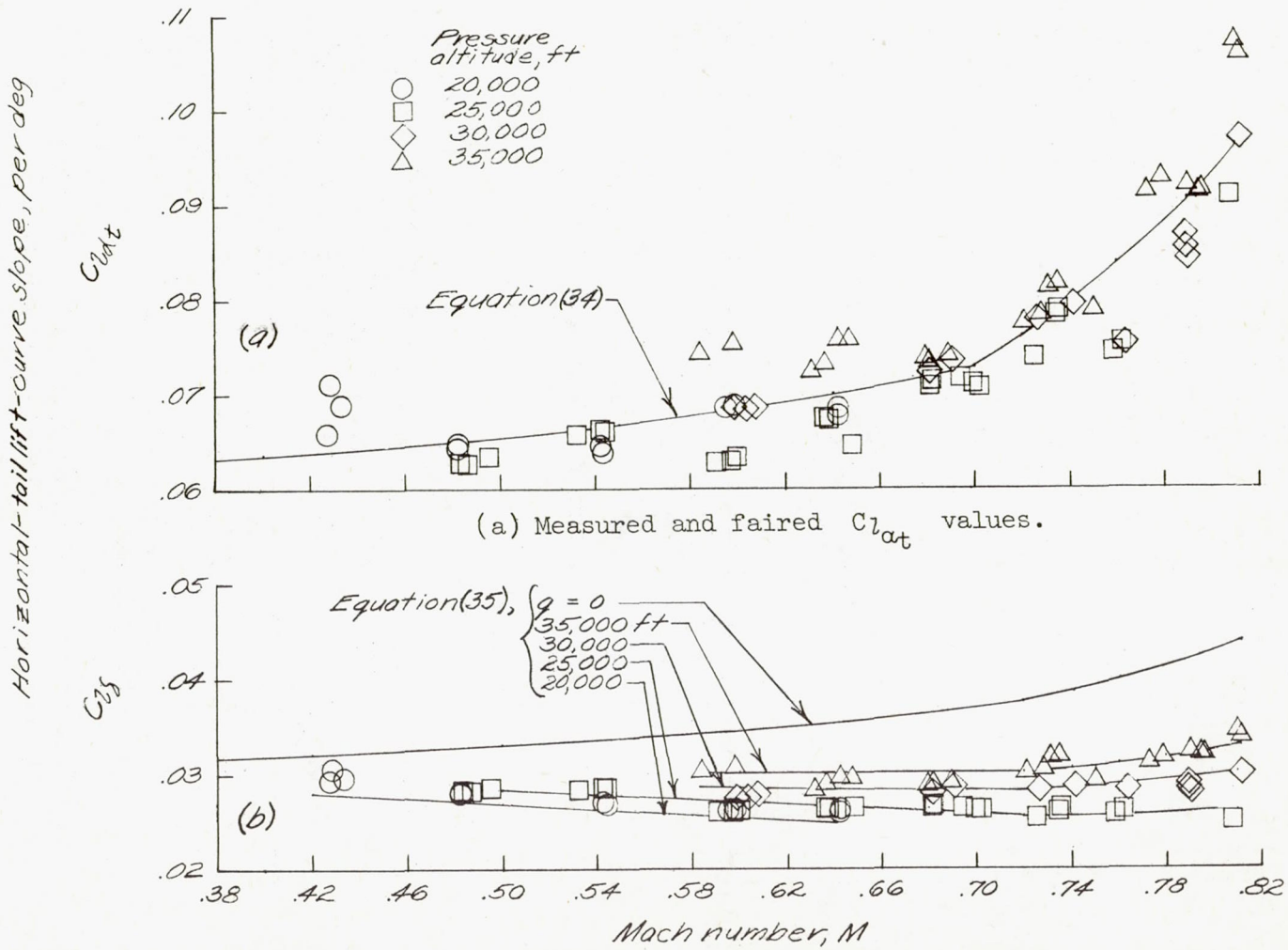


(a) Maneuver of figure 3.



(b) Maneuver of figure 4.

Figure 5.- Comparison of measured aerodynamic tail-load time histories with those calculated by equation (33).



(a) Measured and faired $C_{l_{\alpha_t}}$ values.

(b) Measured and faired C_{l_δ} values.

Figure 6.- Variation of horizontal-tail lift-curve slopes with Mach number.

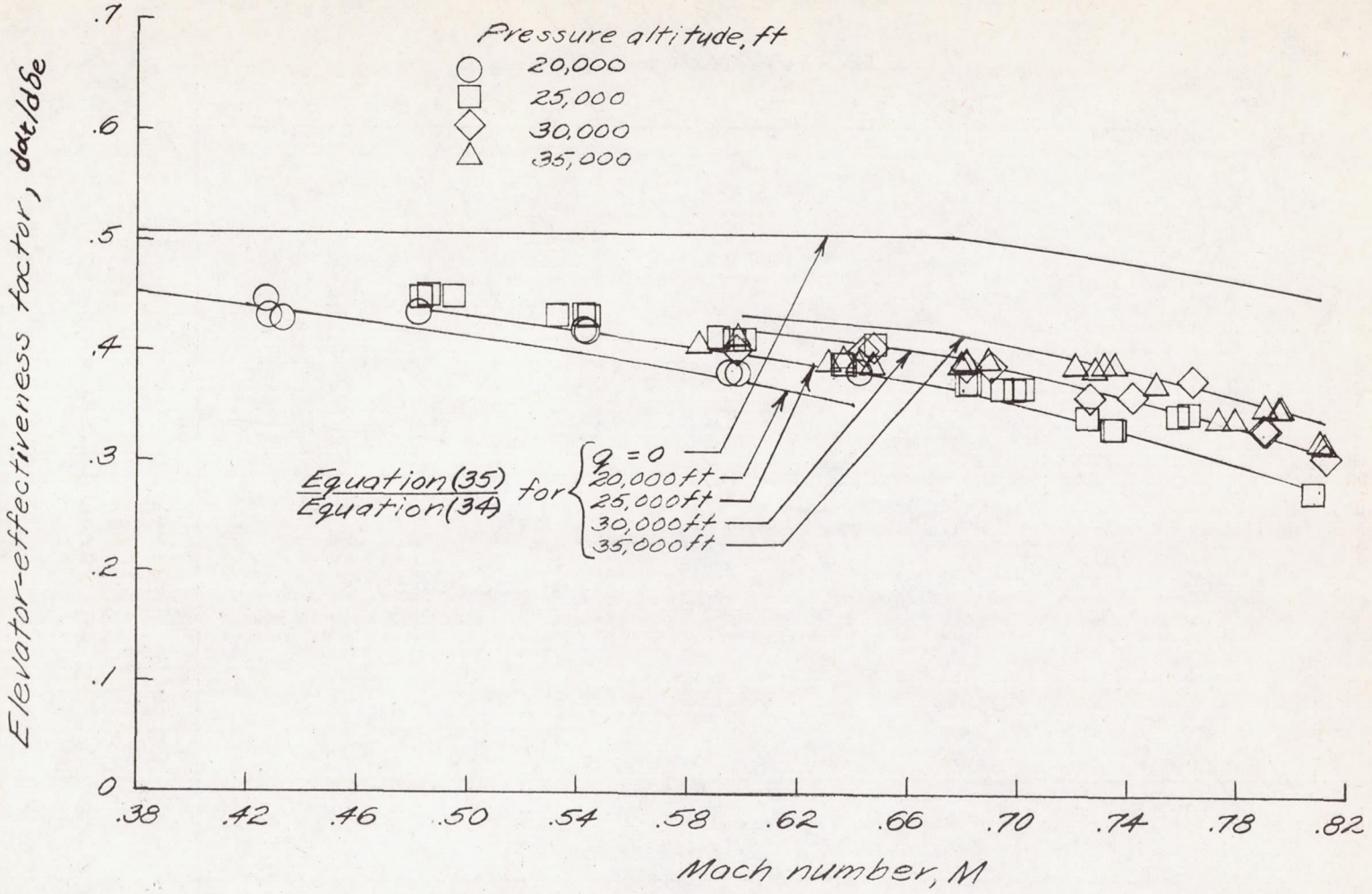


Figure 7.- Variation of horizontal-tail elevator-effectiveness factor with Mach number and dynamic pressure.

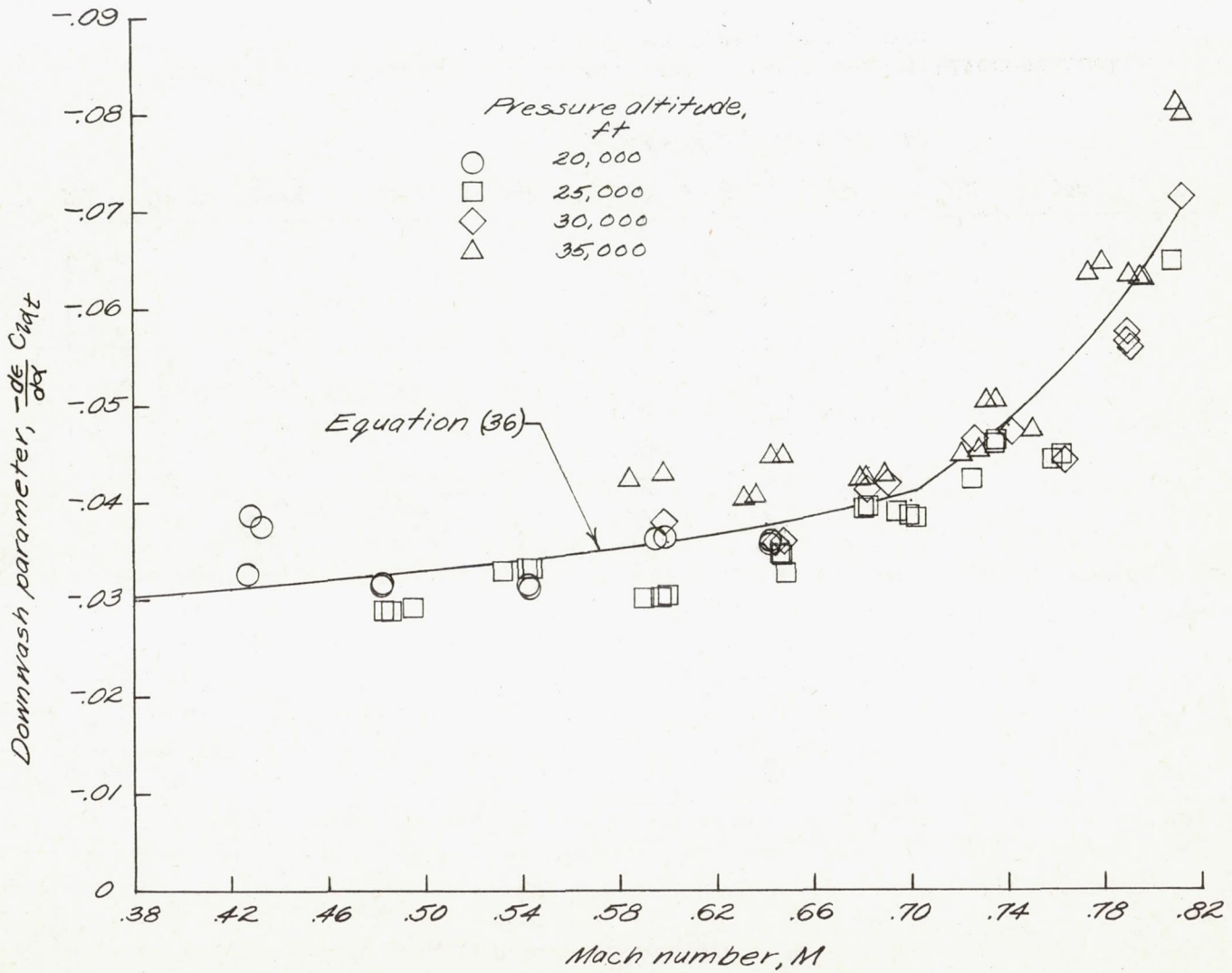


Figure 8.- Variation of downwash parameter $\frac{-d\epsilon}{d\alpha} C_{l_{\alpha_t}}$ with Mach number.

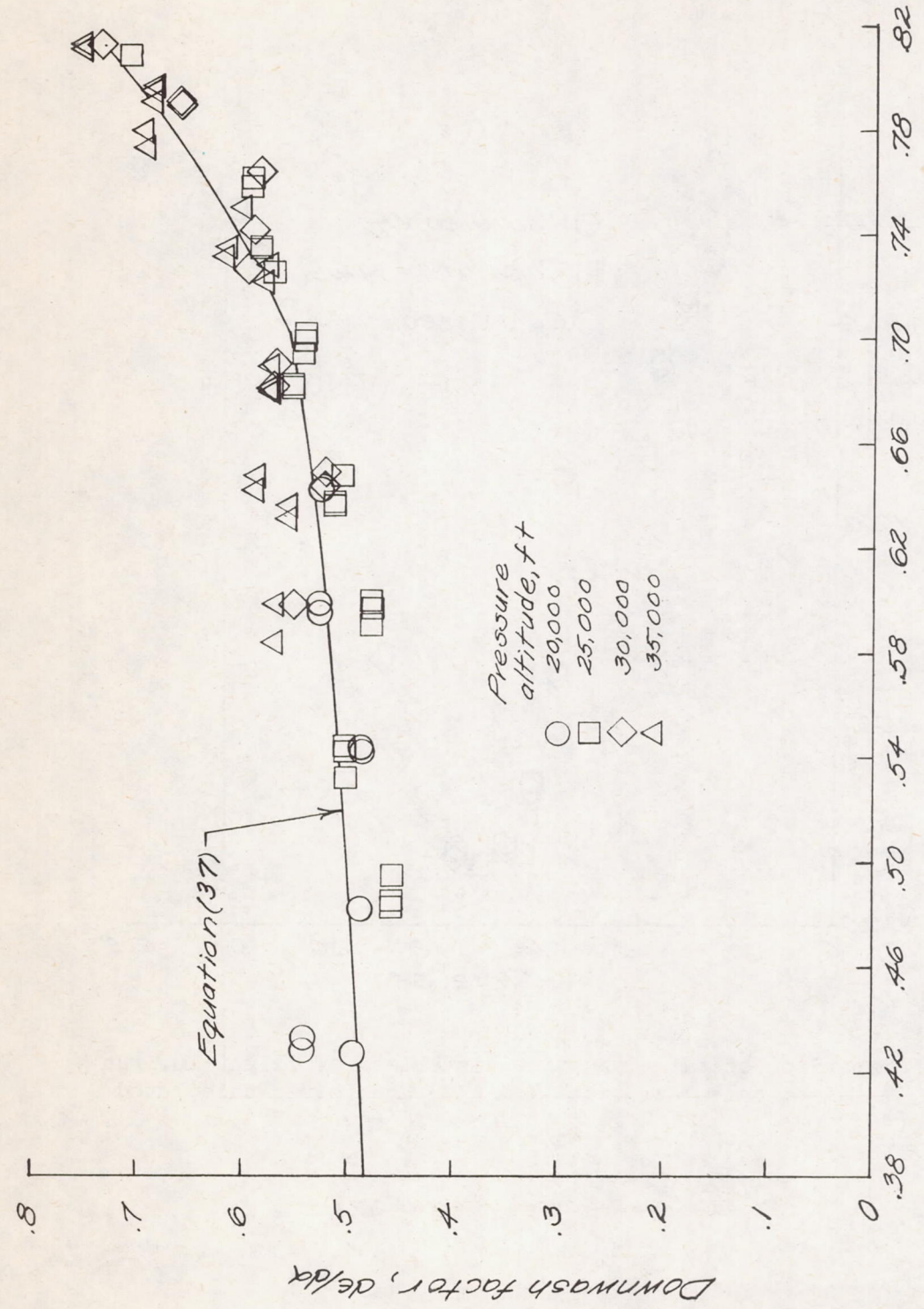


Figure 9.- Variation of downwash factor $d\epsilon/d\alpha$ with Mach number.

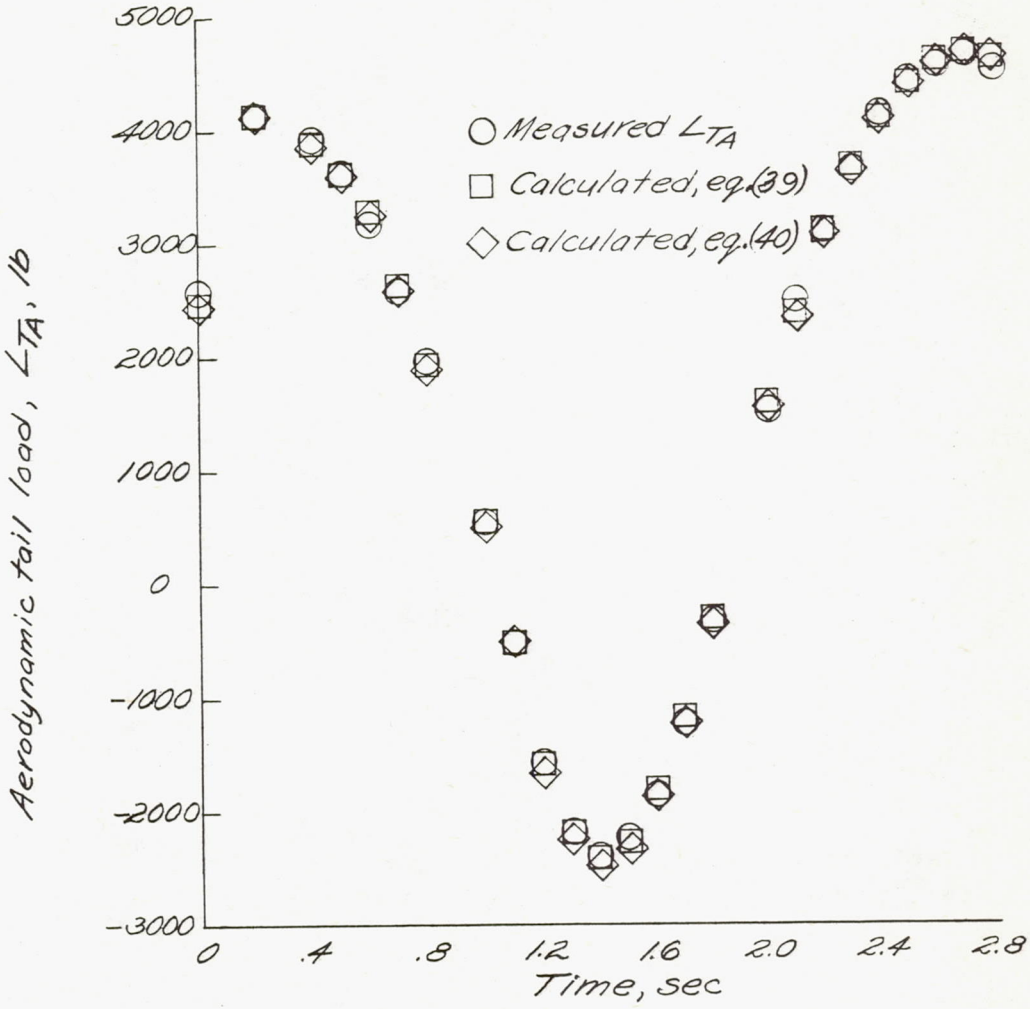


Figure 10.- Comparison of tail-load time histories for flight 10, run 7; measured, unfaired calculated equation (39) and faired calculated equation (40).

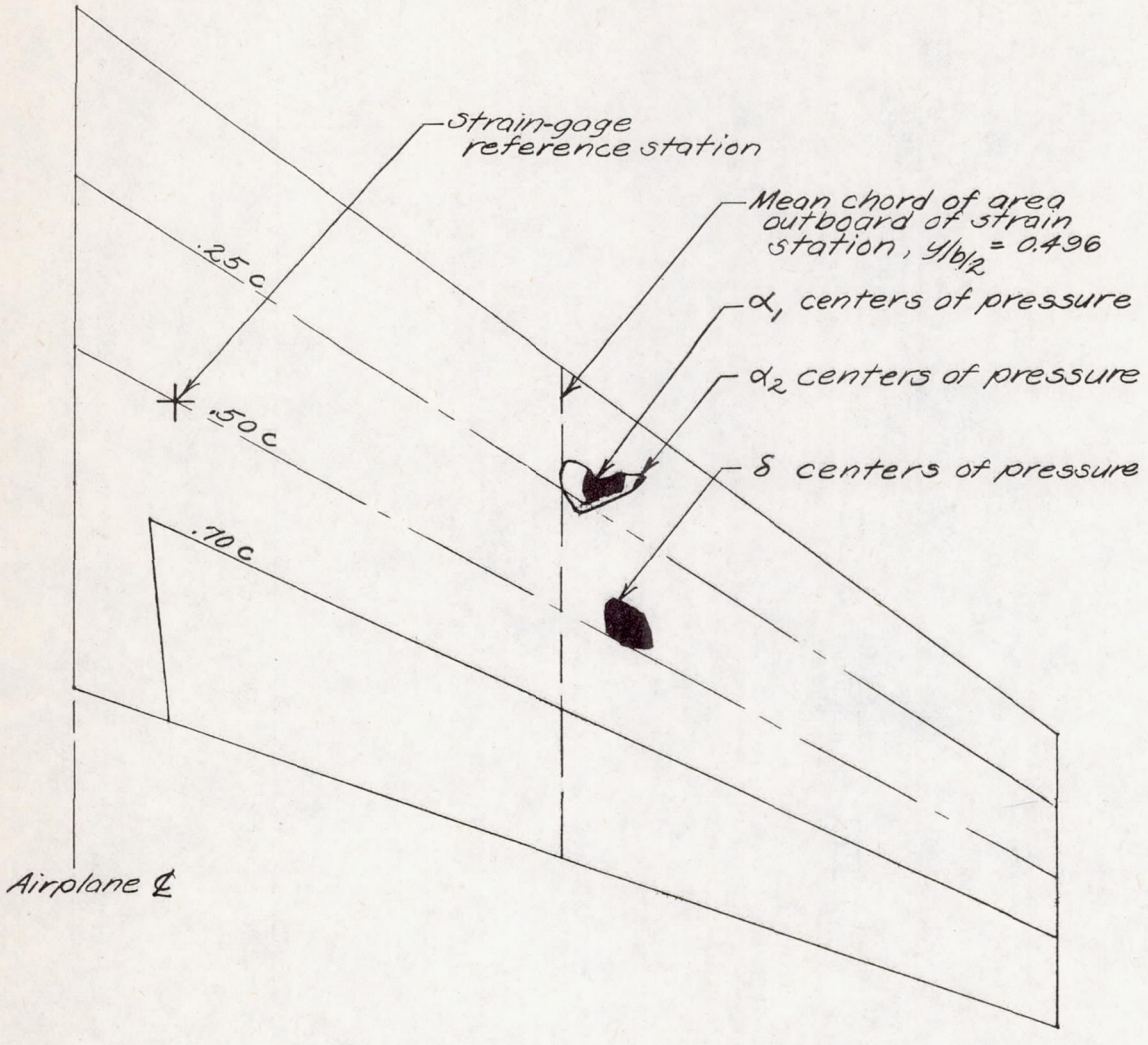


Figure 11.- Measured center-of-pressure locations for horizontal tail.



Figure 12.- Variation of tail pitching-moment coefficient due to elevator deflection with Mach number.

NACA - Langley Field, Va.